Universidade de Aveiro
Ano 2015

Departamento de Química

Antoine LOPEZ

Desenvolvimento de novas bio-espumas sustentáveis preparadas por polimerização em emulsão de Pickering

Universidade de Aveiro Departamento de Química
Ano 2015

Antoine LOPEZ

Desenvolvimento de novas bio-espumas sustentáveis preparadas por polimerização em emulsão de Pickering

Novel bio-foams obtained by Pickering emulsion polymerisation

Dissertação apresentada à Universidade de Aveiro para cumprimento dos requisitos necessários à obtenção do grau de Mestre em Ciências e Engenharia de Materiais, realizada sob a orientação científica da Doutora Carmen Sofia da Rocha Freire Barros, Investigadora Principal do CICECO e do Departamento de Química da Universidade de Aveiro e da Doutora Andreia F. Sousa, Investigadora de Pós-Doutoramento do CICECO e do Departamento de Química da Universidade de Aveiro.

O júri

Presidente

Doutora Ana Margarida Madeira Viegas de Barros Timmons
Professora assistente do Departamento de Química da Universidade de Aveiro

Doutor Jorge Fernando Jordão Coelho
Professor assistente do Departamento de Engenharia Química da Universidade de Coimbra

Doutora Carmen Sofia da Rocha Freire Barros
Investigadora Principal do CICECO e do Departamento de Química da Universidade de Aveiro

Agradecimentos

First of all, I would like to thank professor Carmen Freire, my supervisor, for giving me the chance to have an internship in her team and Andreia Sousa for working with me as my co-supervisor. I want to thank them both for everything they taught me, their availability and their involvement in the thesis.
I would also like to express gratitude towards professor Silvestre for his advice and availability and professor Barros for her support.
I also thank everyone that helped me and worked with me during these 6 months Ana, Carla, Helena, Nuno, and Ricardo. Especially Professor Artur Silva for his help and availability to perform the UV-polymerisations.
Finally, I want to thank, Louise, Diana, Hannes, Eva, David, Marcio, Manon, Mathieu and all the other colleagues from Erasmus, FAME or from the University of Aveiro, for the support and the fun they procured me. Especially Louise and Diana for working beside me for the 6 months of this thesis, and that must not be easy!

Palavras-chave Cortiça, Quercus suber L., nanocelulose, suberina, lenhina, biopolímeros, espumas, polimerização em emulsão de Pickering.

Resumo

A cortiça tem propriedades mecânicas e físicas únicas, em particular uma elevada capacidade de absorção de energia, elevada fricção, baixa condução acústica e térmica, elevada hidrofobicidade e baixa densidade. Estas propriedades estão relacionadas tanto com a sua composição química como com a sua microestrutura. Neste estudo, inspirado por estas características e morfologia únicas da cortiça, desenvolveram-se novas espumas de origem renovável com elevado desempenho. Adicionalmente, devido à necessidade premente em desenvolver concomitantemente materiais sustentáveis e processos verdes, estas novas bio-espumas foram preparadas seguindo abordagens amigas do ambiente. Em concreto, elas foram preparadas por polimerização em emulsão de Pickering de óleo de soja epoxidado acrilatado (AESO) usando celulose bacteriana acetilada como estabilizante da emulsão. Adicionalmente, seguindo mais de perto a microstrura e composição da cortiça, prepararam-se espumas sustentáveis contendo concentrações elevadas de celulose e foram dados os primeiros passos no sentido destas espumas incorporarem compostos semelhantes à lenhina.

As diversas emulsões preparadas bem como as espumas resultantes foram caracterizadas detalhadamente através de várias técnicas, tais como SEM, microscopia óptica, TGA, DMTA, FTIR, estre outras. Verificou-se que a composição ótima da emulsão água-em-AESO foi estabilizada com 70% de água o que corresponde a uma emulsão do tipo 'High Internal Phase Emulsion' (HIPE). A microestrutura celular das novas bio-espumas foi confirmada por SEM, verificado que dependendo da composição inicial das emulsões (rácio água/óleo) pode-se controlar as dimensões e densidades dos poros e assim ajustar a porosidade à da cortiça. Estudou-se o comportamento térmico das espumas via TGA, podendo-se concluir que elas têm um comportamento semelhante à cortiça. É ainda de realçar que em termos de análise por DMTA, verificou-se que a temperatura de transição vítrea varia entre 30-60 ^{o}C.

Keywords Cork, Quercus suber L., nanocellulose, suberin, lignin, biopolymers, foams, Pickering emulsion polymerisation.

Abstract

Cork material have a very unique set of mechanical and physical properties especially high energy absorption, high friction, low acoustic and thermal conduction, good hydrophobicity and low density. These properties are strongly related to the chemical composition of cork, as well as its honeycomb-like microstructure. In this study, inspired by these unique features, we have developed novel high performance bio-foams. Additionally, due to the urgent need to develop concomitantly sustainable materials and green processes, these novel foams were prepared using environment friendly approaches. In this study novel bio-foams mimicking cork were prepared by Pickering emulsion polymerisation of acrylated epoxydised soybean oil (AESO) using acetylated bacterial cellulose (Ac-BC) as an emulsion stabiliser.

Following more closely cork structure and chemical composition, additional sustainable foams composed of higher concentrations of Ac-BC, were prepared. Also, the first steps towards the incorporation of lignin-like compounds in these foams were done.

Both emulsions and ensuing foams were exhaustively characterised by means of several techniques, *viz.*, SEM, optical microscopy, TGA, DMTA, FTIR, among others. The stabilisation of a 70% high internal phase water-in-AESO emulsion (HIPE) was verified. The cellular structure of the novel foams was confirmed by SEM analysis. It was found that depending on the ratio between water/oil we could tune pore dimensions and density, and hence to approach more closely cork microstructure.

Moreover, the new foams thermal properties, especially in terms of thermal stability, were found to be close to cork behaviour. Furthermore, the mechanical properties of the foams were studied by DMTA, and the glass transition value was found to be between 30-60 ^{o}C.

Table of Contents

List of Figures:

Context

High performance materials combining multiple interesting properties are being more and more investigated. The main objective of this study was to prepare novel high performance bio-foam materials inspired by cork material, and determinate how changing the reaction condition and /or composition tunes the ensuing foam properties.

Moreover, in the past decades the increase of the global environmental awareness associated with sustainability and the crude oil depletion, gave rise to an increase interest in renewable-based materials and eco-friendly processes. In this context, the other aim of this study was to define an environmental friendly process to produce these new bio-based materials that will have the advantage of having a controlled homogeneity and cell size.

This thesis is divided in three main chapters focusing on describing cork and the processes chosen to produce the novel bio-foams, the experiments carried out, and finally the results are discussed in the last chapter.

In order to obtain a high performance material, we aim to mimic the chemical composition and structure of cork. The first section of Chapter 1 (*1.1 What is cork?*) describes cork material structure, composition and its properties. The second section of Chapter 1 (*1.2 Process chosen to prepare the bio-foam*) describes the methodology used to produce the novel composite material. Specifically the Pickering emulsion polymerisation approach is described and different parameters and elements needed to prepare an emulsion are highlighted. Chapter 2 (*2. Experimental part*) details the materials and reagents, the methodologies and characterisation techniques used along this thesis.

The last chapter (*3. Results and discussion*) presents the characterisation techniques that were performed at each steps of the herein presented study, namely SEM, TGA and DMTA, and also describes how the processes were optimised in order to obtain a foam closer to cork's microstructure and composition. This same chapter include also the discussion of these results and ensuing foams.

1. Introduction

The outer bark of cork oak tree is a natural closed cell material, usually simply called cork. Cork has interesting properties, like for example its hydrophobicity, thermal and acoustic isolation properties, energy-absorbing capacity, among others[1]. These characteristics make this natural occurring material suitable for a wide range of fields, including the traditional use in cork stoppers, but also in several modern technologic applications[1]. Among the latter, for example, engineers and researchers have already started to replace asbestos, in thermal isolation applications, by cork as an environmental friendly alternative and as a low specific gravity filler in the thermal isolation of space vehicles [2]. Cork unique properties, together with its high-tech applications, makes it a very inspiring material, this study aims precisely to mimic cork microstructure and chemical composition in order to obtain innovative high performance composite materials.

In the first section (*1.1. What is cork?*), natural cork is described in terms of natural occurrence, and main applications through time, chemical composition, mechanical and physical properties. We will see that cork's uncommon properties are due to multiple factors, including its hexagonal-based polyhedral microstructure. Moreover, its chemical composition is the key to its structure stability and plays a primordial role in its physical properties[1].

Inspired by cork composition and structure, Pickering emulsion polymerisation is the process chosen in the herein presented study to create our new high performance bio-foams. The second section (*1.2 Process chosen to prepare the bio-foam*) describes the physical and chemical principles involved with this type of emulsion.

1.1 What is cork?

Cork is the outer layer of the bark of cork oak tree (*Quercu suber* L.), thus being the tree external protective layer, as illustrated in Figure 1.1. Its growth is a reaction of the tree to the death of the initial phellogen, which can occur by natural accidents (fire, hot or dry periods, bacterial or environmental impact) or by removal of the cork layer (for harvesting).

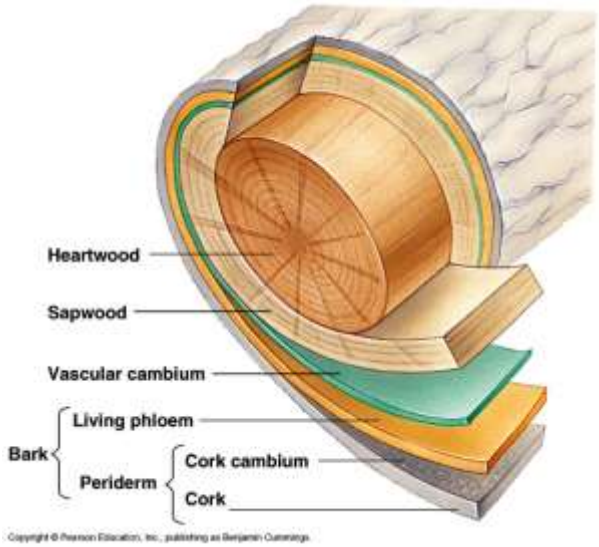

Figure 1.1: ***Schematic representation of Quercus suber L. trunk, depicting cork as the outer of the cork oak bark*** [54]**.**

The next paragraphs are dedicated to describe cork material; first a brief overview about cork's growth (*1.1.1 Formation and growth*), afterward to give its history, production and applications (*1.1.2 History, production and applications of cork*), its structure and chemical composition (*1.1.3 Structure of cork tissue* and *1.1.4 Chemical composition*), and finally, to describe its mechanical and physical properties.

1.1.1 Formation and growth

The western Mediterranean basin is the cradle of cork oak forests due to cork oak environmental specific needs. Portugal is the main cork producer with 49.6% of the world annual production [3] (Figure 1.2).

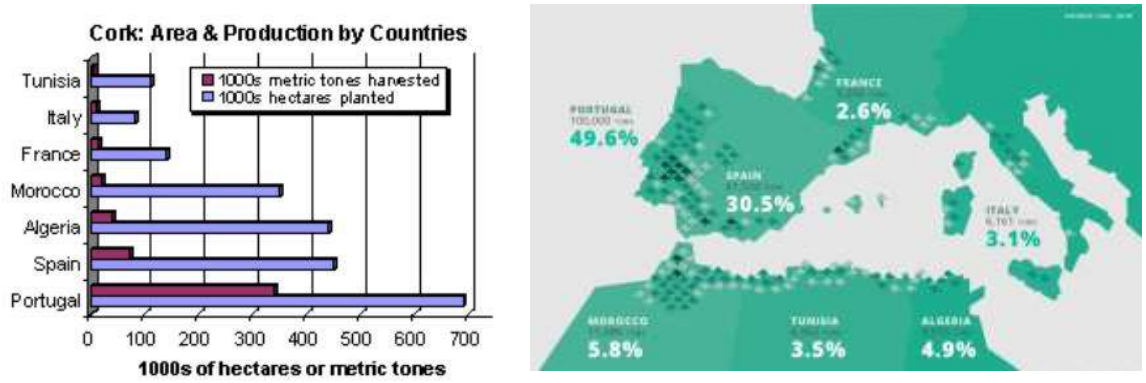

Figure 1.2: ***Production of cork and quantity of cork oak planted*** **(source: FAO 2010).**

Cork industry is considered as environmentally friendly [4,5], for example 83% of the cork oak trees harvested in Portugal are of pure stand (about the same ratio in Spain). Furthermore, these trees can live about 200 years and are not cut down to harvest the cork. It takes approximately 10 years for the cork layer to grow back thick enough, about 4 mm per year, to be harvest again. We can see in Figure 1.3 a picture of the harvesting of cork oak's bark.

Figure 1.3*: Harvesting of cork layers is usually made by hand after the cork oak tree has been meticulously chosen.* [3]

Structure of cork oak's tree can be divided in two parts: the inner part (the xylem) and the outer part (the bark). Cork layers grow as the external part of the bark, as what is usually called periderm. Contrary to other tree species, the outer protective layer of cork oak has specific properties that make it possible to produce cork in a sustainable way.

When the outer wall is damaged, for example after harvesting, the first phellogen (called traumatic periderm) forms very quickly during the first year after the damage. Under this first protecting layer, the phellogen start growing a high number of cork close packed cells at a regular speed and as a regular cylinder around the vertical axis. This makes the cork tissue very homogeneous around the axis. But also because of the transversal growth, the cells have a specific orientation in their shape (*1.1.3. Structure of cork tissue*). However, the growth rate decreases during harvesting years. Going from about 6 mm per year in the first year to hardly more than 2 mm after eight years [1]. Even so, the growth rate increases during the early years of the trees but once they have reached their maturity, this rate decreases every year. For example on a 140 year cork oak, until its 70^{th} year the cork thickness increases from 1,8 cm to almost 3 cm every year, before decreasing to 1,5 cm growth during its 140^{th} year[1]. This irregular growth rate during its life affects the homogeneity of the cork layer, and could affect its properties too. This variablility is a drawback associated to natural material, as cork is.

1.1.2 History, production and applications of cork

Cork has a long history, dating its first uses to the ancient times where it was used as such, as raw material, but with the advances of science, its processing changed in order to enhance some of its properties. In the present section we will shortly describe cork history and the progress in production and applications as years went by.

In Egyptian time, cork was used as stoppers for casks. Ancient Greeks added to this use fishing net floats and sandals. Afterwards, Romans widely used cork in a variety of ways, including life jackets for fishermen, still focusing on its non-wettability and low density. Aware of cork's low thermal conductivity, Mediterranean homebuilder built cottages, for hundreds of years with cork roofs and floors to keep out summer heat and

winter cold, and to provide a soft walking surface[1].

Since the ancient times of Greeks and Romans until today, cork is used as bottle stopper material; in order to produce this bottle stoppers cylinders are cut out of raw cork tissue. This process generates a lot of waste material in between each bottle stopper. However, in the late 19th century, a German company used this cork leftover, by adding a clay binder to cork particles and producing sheets of cork composites for use as insulation materials[6]. This technique was improved a few years later by removing the clay binder and creating a pure-cork agglomeration out of waste material by subjecting cork particles to heat and pressure. This started a new area of improvement to create cork composites. Many other techniques have been developed to produce cork-based material with a variety of properties and uses [7].

Figure 1.4 summarises some of the applications of cork materials. As already referred, the most well-known application for cork material is as bottle stoppers, but cork is also used in multiple other fields. For example, white agglomerates of cork (obtained by grinding virgin cork) can be used as footwear, protective helmets, life jackets and floats, fishing rod handles, handbags and briefcases, and even as fabric for clothing and paper. Its high energy-absorption property makes it useful for industrial engines as mechanical joints or anti-vibration material. Black agglomerate (made from cork waste which is ground and heated at high temperatures) is used above all for thermal, acoustic, and vibration insulation purposes. These grains of cork can also be combined with rubber (rubbercork) and used as an elastic and strong material for automotive and electrical industries. In the building industry, sheets of cork composites are used as covering for floors and walls taking advantage of the thermal isolation properties and the hydrophobicity of cork.

Figure 1.4: ***From left to right: cork stoppers, white and black grains for agglomerates, rubbercork and cork floor*** [3]**.**

1.1.3 Structure of cork tissue

Cork tissue is created layer by layer under the phellogen layer. Its cells are empty and arranged in a close packed way, without intercellular void. In that way cork tissue is, by definition, a closed cell material, with a mean value of 10% solid fraction. This very low value of solid fraction is associated with cork low density, approximately equal to 120-170 kg/m^3 [1].

As previously mentioned, in section 1.1.1. Formation and growth, the phellogen mother cells create the cork cells. These mother cells have a hexagonal shape base from which they grow the periderm in a circular growth. Basically, cork tissue looks like a honeycomb (Figure 1.5).

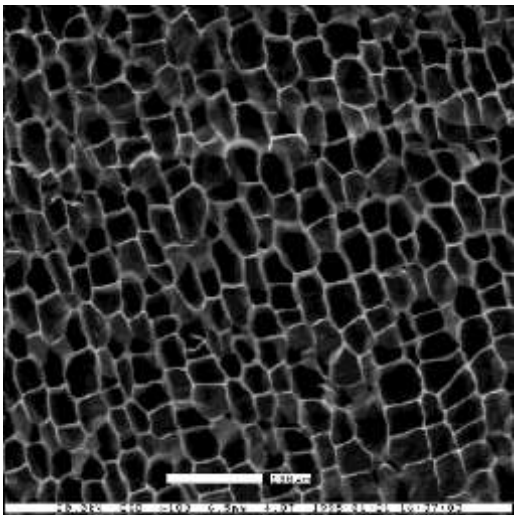

Figure 1.5*: SEM pictures of the honeycomb structure of cork tissues (SEM images from The Museum of Palaeontology of The University of California at Berkeley and the Regents of the University of California).*

Cork cells are, thus, a hexagonal prism with its face in the axial-tangential plan and with its axis symmetry on the radial axis. Its hexagonal base has in average edges of 20 µm, and the average length of a cork cell is 40 µm. The average thickness of a wall is about 1 µm. The shape of the cork cells is sketched in Figure 1.6.

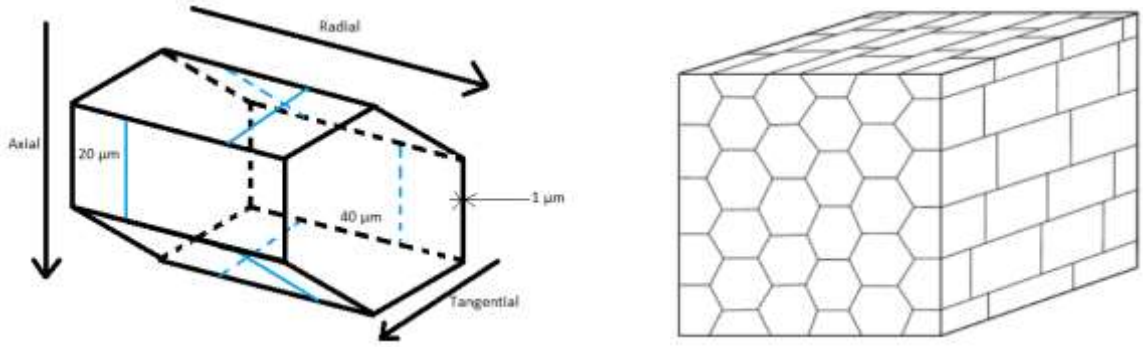

Figure 1.6*: On the left: Sketch of a cork cell. The black lines represent the edges of the cell and the blue lines represent the edges of other cork cells surrounding the sketched cork cell. Notice that delimited by both blue and black edges we can count 14 faces of contact between cork cells (Telwin polyhedron). On the right: cell arrangement in typical cork tissue* [1].

The radial growth of cork cells creates an intrinsic anisotropy. Besides the obvious radial axis symmetry of the hexagonal prisms inducing a shape-anisotropy, it creates a specific chemical repartition (which will be explained in the following section *1.1.4 Chemical composition*). These anisotropies play a primordial role in the various properties of cork.

Cork is an extremely complex closed-cell material, and its properties change along the radial growth axis during the year. Each of its particularities and changes has an effect on properties of the material.

This honeycomb like structure explains the well-known energy absorption of cork material in terms of mechanical compression, thermal conduction and acoustic conduction, this will be explain more in details in the section 1.1.5 (*Mechanical properties of cork*) and (*1.1.6 Physical properties*).

1.1.4 Chemical composition

For a material with such a low density and such a complex structure, the fact that the cells can keep their shape without collapsing is unique. We have to learn more about the chemical composition of cork in order to explain this steadiness. Some of cork properties, like for example its chemical inertness, are only due to chemical composition. But most of its properties result from both chemical composition and architecture of the cell wall.

As any other wood tree, cork cell wall is constituted by two types of compounds: structural and non-structural compounds [1]. The formers are polymeric macromolecules responsible for the microstructure of cork; meaning that if we remove them the cell would collapse, and in that way they are responsible for most of cork properties. The non-structural compounds are, essentially, low molecular weight organic compounds or mineral, not having an important impact on structural behaviour of cork, mainly influencing its chemical and biological behaviour.

In this study we will focus on cork's structural components, because the non-structural components represent only 2-3% [8] of cork's global chemical composition. Among the structural compounds of cork material, we can quote in decreasing order of weight percentage (wt. %): suberin (up to 58 wt. % [9] of cell wall composition), lignin (*c.a.* 22 wt. % [9]) and polysaccharides (*c.a.* 18 wt. % [9]). The ratios of these compounds are represented in the Figure 1.7, with the comparison of wood and cork of cork oak.

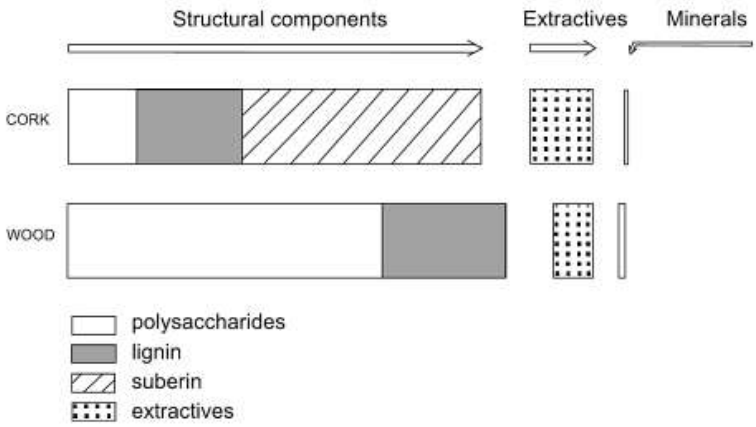

Figure 1.7*: Schematic representation of the proportion of the structural chemical components of cork and cork oak wood* [1]**.**

Figure 1.8 shows a model, proposed by Sitte[10], about the structure of cork oak cell wall. In the outer layer (the primary wall) are lignin and cellulose linked to suberin polyphenolic domain and finally suberin polyaliphatic domain. The relations between these components will be detailed in the following sections.

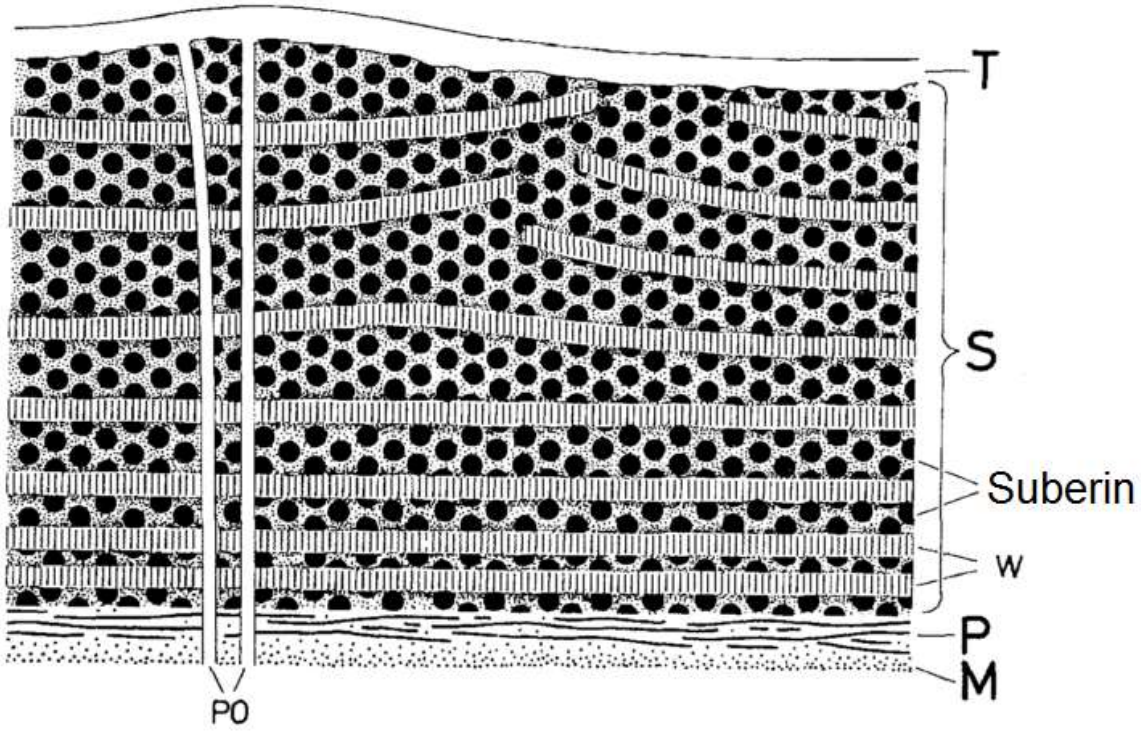

Figure 1.8*: Model, proposed by Sitte, for the topology of cork cell walls*[10]*. (T) tertiary wall, (S) secondary wall, (W) waxes and suberin, (P) primary wall, (M) medium lamella, (Po) pore.*

The following subsections are dedicated to a brief description of cork suberin (*1.1.4.1*), lignin (*1.1.4.2*) and polysaccharides (*1.1.4.3*) in order to understand better the effects of their chemical composition and architecture on cork's properties, in section *1.1.5. Mechanical properties of cork* and *1.1.6. Physical properties*.

1.1.4.1 Suberin

In the literature, there are reported suberin amounts in cork oak bark ranging from

37,8 % [9,11] up to 60-62 % [8,12], therefore suberin is the most important component of cork tissue. But, besides being the most abundant component of cork, suberin is the only structural compound of cork that is not present in the wood of cork oak (Figure 1.7). It takes part in the stability of the structure of cork cells, as it has been experimentally observed the collapse of the cells after partially removing it [9].

Suberin is also found in other plants and even in different morphological parts of the plants[13]. For example, this biopolymer is present in the underground part of plants (*e.g.* tuber phellem of potato) or in the wounded upper part of the plant, acting as a protective barrier between the plant and the environment [14] and, in some plant cells, providing water retention [15]. In the last decade, the definition of suberin has been actively discussed. In the following section we will describe the broad-accepted model suggested by Bernards [15].

According to this model "suberin is a natural aliphatic–aromatic cross-linked polyester" [13]. It is indeed composed by two domains: the suberin polyaliphatic domain and the suberin polyaromatic (or poly(phenolic)) domain, denoted by SPAD and SPPD, respectively [15]. Several studies showed that SPAD and SPPD represent more or less 50% each of suberin [16,17]. The two suberin domains are cross-linked by ester linkages and glycerol links. The importance of glycerol in the linkage and the chemical architecture has been taken into account very late in the study of cork suberin, and there is still a lot to determine about its role in suberized cells. Graça and Pereira [8] studies reported up to 14% of glycerol in their chemical analysis of cork suberin.

There were a huge number of studies [8,10–12,14,17,18] focused on determining the composition of suberin, however depending on the method used and the sensitivity of the analysis devices, and/or the sample analysed, the identified compounds, but especially their amounts changed. Gandini summed-up most of these studies in 2006 [13]. Anyway, all the results tend to have the same order of magnitude for the amount of each family of compounds in cork suberin.

The suberin polyaliphatic domain is mainly composed of long carbon chain fatty acids essentially ranging from C16 to C26. Typically, in decreasing order of weight percentage magnitude there is: ω-hydroxyalkanoic acids (representing up to 62% of suberin monomers [18]), then α, ω-alkanedioic acids (representing up to 46% [17]), and finally

aliphatic acids and fatty acids represent around 10 to 15%, respectively[12]. These long carbon chains (C16 to C26) are associated to cork tissue flexibility and hydrophobicity[13], this suberin domain is also named waxes of suberin[14]. Some of the most abundant compounds found in the SPAD are represented in Figure 1.9. In the chemical architecture of suberin, all these monomers are linked within the SPAD, typically by ester links, creating the so-called suberin oligomeric blocks [14] .

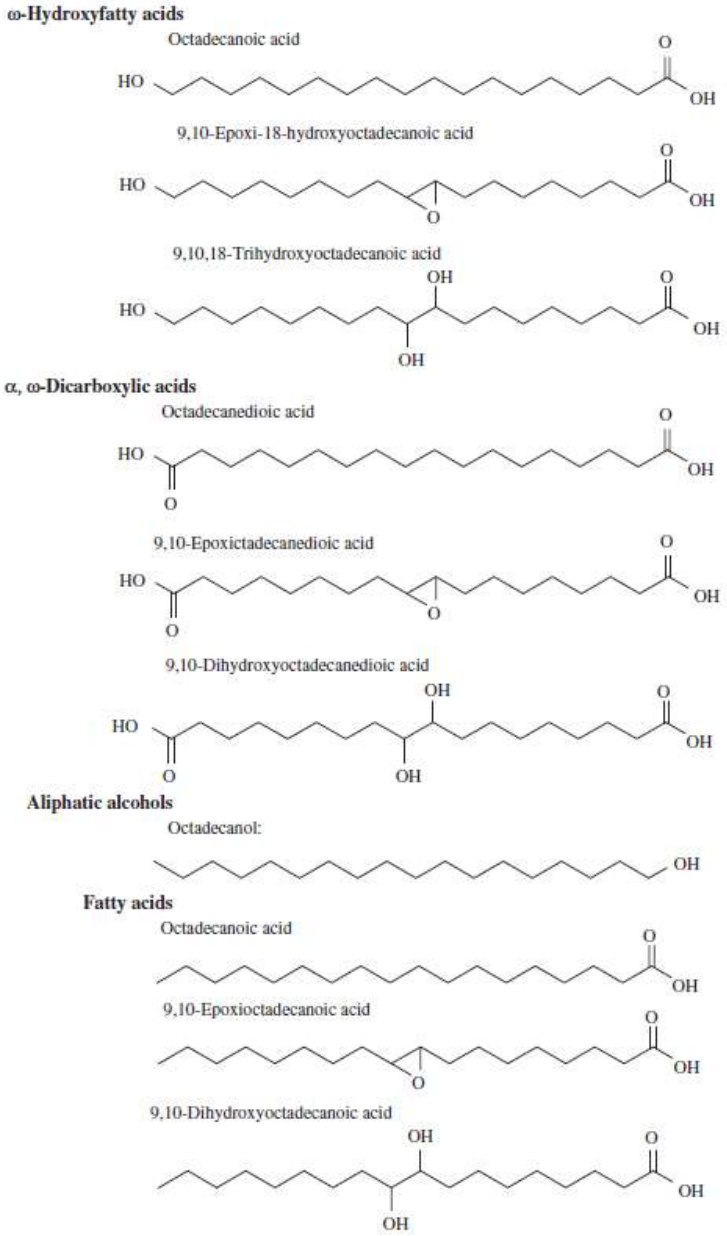

Figure 1.9*: Representation of typical monomers composing the SPAD of cork, organised from top to bottom in the lowering concentration order* [13]**.**

For a long time, it was discussed the existence of suberin polyaromatic domain [19], also called suberin polyphenolic domain; it was considered at first that lignin had the role of the aromatic domain in suberized cells. However, several studies [20–22] have shown "that suberized tissues contain a significant amount of hydroxycinnamic acids and a relatively smaller amount of monolignols than that expected for a lignified tissue"[15] , this discover have trigger the definition of this domain of suberin: the SPPD. As previously mentioned, the polyaromatic part of suberin is composed by cross-linked hydroxycinnamic acids, the phenolic precursors of this domain are represented in Figure 1.10.

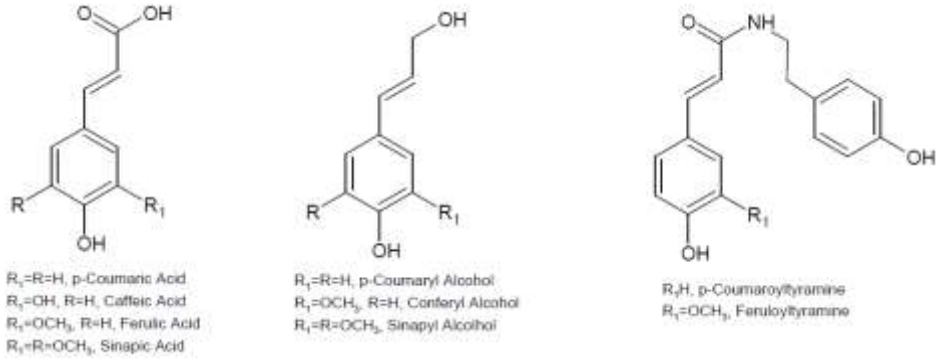

Figure 1.10*: Phenolic precursors detected in the SPPD domain of cork* [13]**.**

This domain is segregated from the aliphatic domain of suberin but is covalently bounded to the latter, typically by glycerol units. The SPPD is contained in the primary cell wall of the cork cell, which means that it is also the link between suberin and lignin in the architecture of the cell wall (as represented in Figure 1.8). The linking between SPPD and lignin is still under study but some hypotheses consider it to be fused with lignin-cellulose matrix [10,13,23,24]; Gandini stated in 2006[13]: "This lignin-like suberin fraction, at least in the case of *Q. suber* cork cells, is embedded (not spatially segregated) in the lignin-carbohydrate matrix of the primary cell wall". These domains mainly composed by cyclic carbons monomers are taking part of the rigidity of cork material and so helping the steadiness of the structure of the cells.

Based on all these observations and the studies quoted in the previous paragraphs, Bernards proposed in 2002[15] a model of the chemical architecture of suberin embedded in the cell wall topography, this model is represented in the Figure 1.11. We can see the SPPD

belonging to the primary cell wall and the SPAD is part of the suberin lamellae (Figure 1.8).

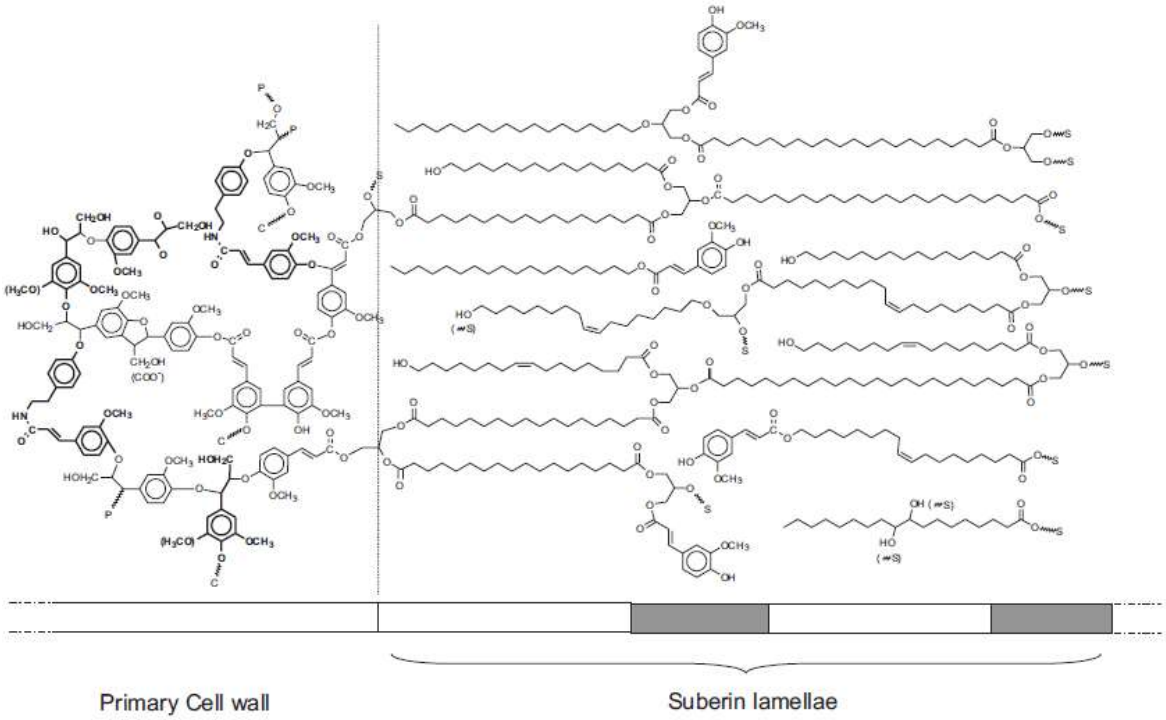

Figure 1.11*: Suberin structure proposed by Bernard in 2002, we can see the aromatic domain of the suberin as the primary cell wall, and the aliphatic part as the lamellae suberin.* [11] ***We can notice the presence of phenolic functions in the aliphatic domain of suberin underlining a complex 3D structure where these parts are fold and linked to the aromatic domain of suberin.***

In conclusion, suberin is the main (>50%) [9] structural polymer of cork cell walls. It is composed of a cross-linked aliphatic domain (long carbon chains (50% of suberin)[16,17]) which give the flexibility of the cell wall and an aromatic part (mainly acids-based moieties like hydroxycinnamic acids) linked by esterification, ether linkage and glycerol cross-linking to the aliphatic domain, giving their rigidity to the cell walls.

1.1.4.2 Lignin

It has been noticed also the occurrence of a second type of polyaromatic cork domain, the well-known lignin-fraction. Lignin is the second most important component of

cork material, representing around 22 wt% of the cell walls mass[8]. As it has been shown for suberin, if lignin is removed from the cell wall, the cork cell collapsed [9]. In that sense lignin is also a structural polymer of the cork cell wall.

Lignin is the result of "the dehydrogenation of phenolic precursors, like coniferyl alcohol (Figure 1.12), via a free-radical coupling process" [25]. Cork lignin is mainly (95%) composed of guaiacyl type lignin that is mainly derived from coniferyl alcohol, as in softwoods. Radical-radical coupling between coniferyl alcohol can be done by various bonds. The different coupling between the phenolic precursors units and the aromatic carbon ring structure give to lignin a rigid chemical structure which contributes to the mechanical properties of cork material.

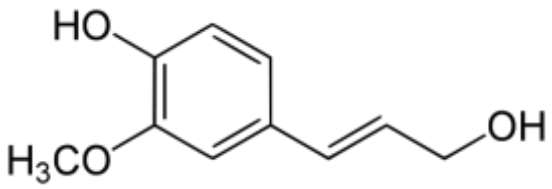

Figure 1.12*: Coniferyl alcohol.*

As shown in the Figure 1.8 and described in the previous section, lignin is a component of the primary cell wall: composing the matrix in which the polyaromatic domain of suberin is embedded. Other components of this matrix are polysaccharides.

1.1.4.3 Polysaccharides

The third structural polymers of plant cells are cellulose and hemicelluloses, representing around 20% of dry mass weight in cork [9]. Polysaccharides are quite less abundant in cork than in wood or in other bark tissues (around 70%) [9]. Like for suberin and lignin, the structural importance of polysaccharides, was shown by removing them from cork cell and observing the collapse of the cells [9].

Cellulose is a linear homopolysaccharide of glucose molecules linked through β-1-

4 glycosidic bonds (Figure 1.13). In cork cell, cellulose (approximately 10 %wt) is located in the primary (external wall) and tertiary (intercellular wall) walls.

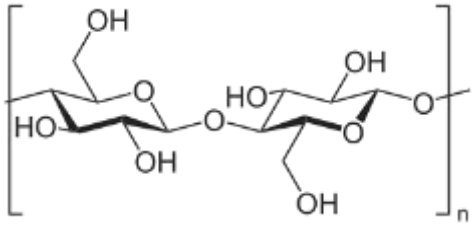

Figure 1.13*: Cellulose unit cell, with a β -(1-4) glycosidic bond.*

1.1.5 Mechanical properties of cork

The preceding description of the geometrical and chemical structure of cork is of upmost importance due to the fact that they have an enormous impact on the properties of this material including the mechanical properties described in this subsection.

We have to keep in mind the anisotropy of cork cells during all mechanical tests, even if the cell may answer in the same way to tangential and axial stresses, the radial response will surely be different, as we can see in the curves of tensile test shown in the graph of Figure 1.14[6].

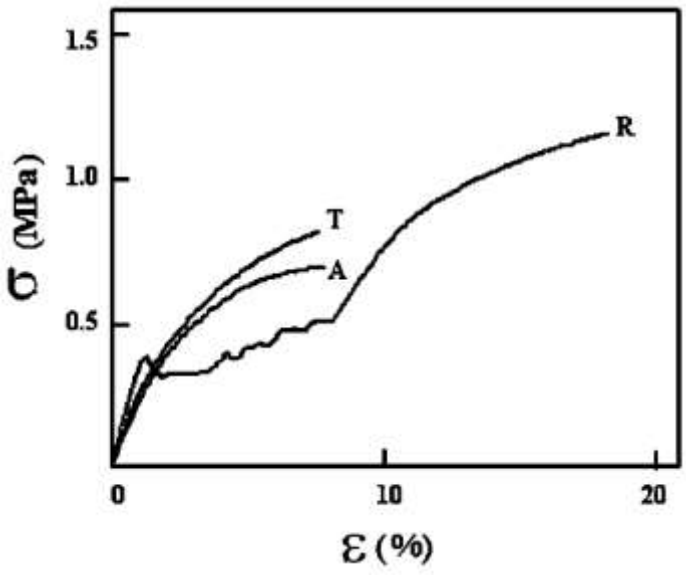

Figure 1.14*: Stress–strain curves in tensile tests for cork, in all directions: T, tangential; A, axial; R, radial* [6].

Typically, the stress *vs.* strain (σ *vs.* ε) curves of cork are divided in three regions, as expected for cellular foam materials response to compression, and as illustrated in the curves of Figure 1.15[6]. At low strains, inferior to 7% [6], is observed a relatively abrupt yielding corresponding to the elastic deformation of the cells, typically with a stress equal to *c.a.* 0,25 MPa in axial (A) and tangential (T) directions and *c.a.* 0,5 MPa in the radial (R) direction[1]. Increasing the strain, a second region is reached, corresponding to the elastic buckling of the cells (up to 50%[6] strain, for 0,7 MPa in T and A directions and 1,2 MPa in radial direction)[1]. The cell walls can buckle without fracture or permanent damages of the walls. Finally, at higher strains, the last region corresponds to a densification of the cork resulting from the collapsing of the cells. A maximum densification is observed up to 85% strain (corresponding to more than 3 MPa[1]). Notwithstanding, even after total densification of the cork tissue, it was not detected fracture or fissures in the cell walls [6].

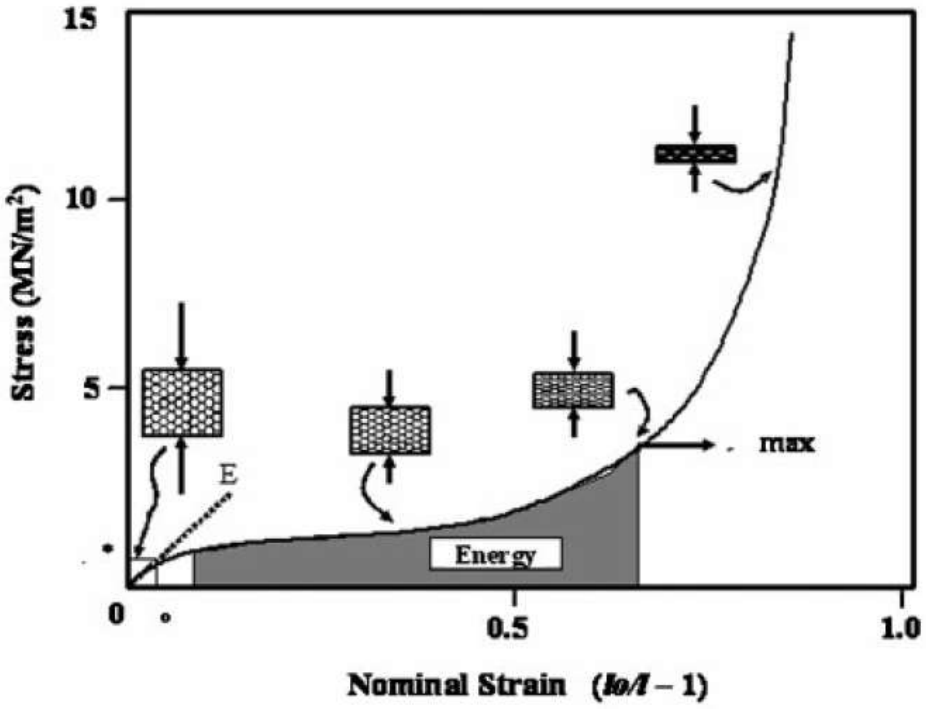

Figure 1.15*: Typical compressive stress vs. strain curve of cork* [6]**.**

As we have seen in the compression strain measurement, cork cells have the capacity to bend without breaking, originating a plateau in the stress-strain compression curves and it explain also the very low Poisson coefficient of cork in radial compression. Instead of transferring the force from a cell wall to the cell walls perpendicular to the force, the walls absorb the energy by collapsing. In non-radial direction, the Poisson coefficient is even negative, and by applying the force on the sides of the hexagonal base, these phases are squeezed which increase their radial dimension.

1.1.6 Physical properties

In terms of physical properties, both cork chemical composition and structure play an important role. Cork has a low wettability to polar liquids (contact angle of 85° with water)[1] but it has a high affinity with non-polar liquids, which can be easily understood having in mind its chemical composition, especially the nature of its main component, suberin. This affinity between cork and non-polar (macro)molecules can be interesting in composites processing.

Cork has also a high friction due to its high energy absorption capacity in compression and the high surface roughness.

Its low solid fraction and hollow cell-like architecture is associated with cork's very poor heat transfer properties by absorption of gas convection and heat radiation.

1.1.7 Interests of cork

As mentioned earlier in this chapter, cork is a low density, closed-cell, cellular material with a solid fraction of around 10 to 20%. Its growth takes several years. Furthermore, cork has several desired properties, like for example its hydrophobicity, heat and acoustic isolation ability, high energy absorption or friction. Cork is not only interesting in terms of mechanical performance, but also its physical and thermal properties are highly sought-after. In fact, apart from its traditional application in the production of cork stoppers, cork is starting to be implemented in several new technologies and high-tech

fields.
Cork is a very complex material. This complexity can be seen in multiple ways: structural arrangement of the mater, chemical composition, arrangement of the components in the cell walls in order to sustain the microstructure.
It is also recognized that the mechanical and physical properties of cork are closely linked to its high complexity.

This study aims, precisely, to obtain an innovative bio-based material, with interesting properties, by mimicking cork composition and morphology. Hence, in order to achieve such a complex biomaterial we had to choose chemical processes that could create a porous material based on biopolymers, in which the cells are close packed and homogenous, and more, that uses environmental friendly conditions.

1.2 Process chosen to prepare the bio-foams

Among the wide number of bio-based porous materials existing today, some of the most interesting ones are those based on cellulose, and more recently on nanocellulose due to their properties and multiple applications, like for example, immobilization of enzymes [26], thermal and acoustic insulation materials, also in pharmaceutical and biomedical fields[27]. These porous materials can be prepared by several approaches, probably one of the most popular is by polyurethane foams synthesis, however, the increase of environmental awareness shifted the researches towards greener processes and green materials. Among those, cellulose is a bio-material easy to produce and to use. Thus in 1931, S. Kistler [28] created new cellulose-based foams, specifically cellophane aerogels, this date marks the beginning of the development of a lot of other cellulose aerogels using distinct methodologies.

Inspired by cork composition and structure, the Pickering emulsion polymerisation was selected aiming to create a close cell material. Nanocellulose was selected as stabilizer and Acrylated Epoxidised Soybean Oil (AESO) was selected to create a matrix that mimic

the long chain fatty acids of suberin.

In the following section a background description of this process and the chemical mechanisms behind them will be provided. Firstly, the principles associated with emulsions and emulsion polymerisation will be described, then the specific emulsions chosen for this process, the Pickering emulsions will be explained.

1.2.1 Emulsions

An emulsion is a dispersion of one liquid in another liquid, which are immiscible. There are several examples of emulsions which can be found in food, *e.g.*, vinaigrette, milk, mayonnaise, among many others[29].

Almost all emulsions involve water as one phase and an organic liquid as the other phase. The latter is usually referred to as the 'oil'. Hence, there are two main types of emulsions, *i.e.*, 'oil-in-water' (o/w) and 'water-in-oil' (w/o). In an emulsion, the two liquids stay immiscible, but one of the two phases is dispersed, as droplets, in the second one. The former liquid is called dispersed phase, and the latter liquid is designated by continuous phase. Figure 1.16 [30] shows a schematic illustration of an emulsion.

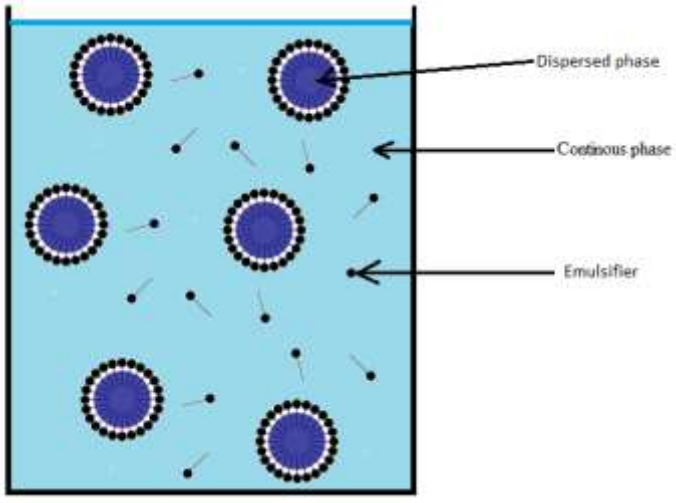

Figure 1.16*: Sketch of an emulsion, here oil-in-water emulsion*[30].

For example, if an oil is dispersed in water without the presence of a stabilizer, the stability of this o/w emulsion tends to be poor[30]. Hence, the oil droplets tend to coalesce.

The introduction of a surfactant in the mixture creates micelles of one liquid, dispersed in the second liquid, stabilizing the emulsion. The separation between the dispersed phase and the continuous one is called the interface. This interface is composed by the emulsifier that is a substance helping the stabilization of the emulsion. They are usually amphiphilic molecules with both hydrophilic and hydrophobic parts, which is why surfactants are good emulsifiers.

1.2.2 Emulsion polymerisation

Emulsions have been used in several applications including the performance of polymerisation reactions, like for example radical or polycondensation polymerisation reactions[31]. As previously described, an emulsion contains two phases and a stabilizer, typically a surfactant. Based on that fact, there is a creation of micelles by one of the two phases which can act as reactors, to have a localized chemical reaction in one of these two phases. This is the principle of emulsion polymerisation, which is sketched in Figure 1.17.

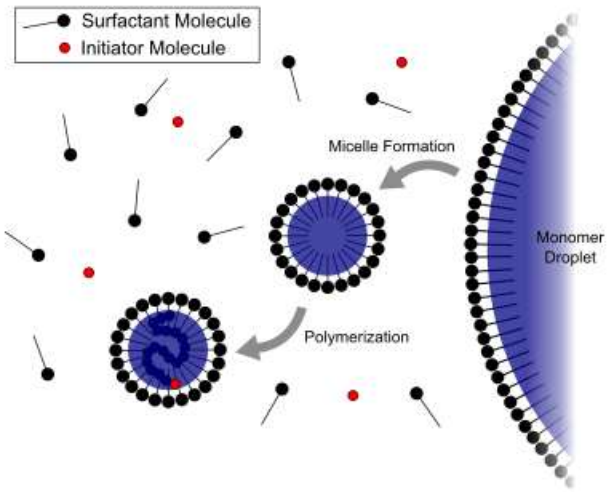

Figure 1.17*: Emulsion polymerisation principle*[30].

For example, in a radical polymerisation conducted in an o/w emulsion, droplets of monomers are dispersed in water. The introduction of a surfactant creates smaller micelles of monomer. Then a water-soluble initiator is introduced. Because the micelles are smaller and in bigger number than the monomer droplets, their surface area is higher, and so the initiator diffuse in the micelles where it start the radical polymerisation. As the quantity of monomer in the micelle decreases, monomers diffuse from the monomer droplets toward the continuous phase, then toward the micelles. This process goes on until all the droplets of monomers have the same size as the micelles.

1.2.3 Pickering polymerisation

In the early 20th century, Ramsden[32] and Pickering[33] observed that the stabilisation of an emulsion occurred not only with surfactants but also with the help of small, micro-sized particles within the interface of the emulsion. Specifically, Ramsden[32] observed the effect of the addition of a clay, while Pickering[33] studied natural "emulsion with insoluble emulsifiers", like cream/milk emulsion or the use of copper sulphate particles as emulsifiers. This type of emulsions took the name of one of the researchers: Pickering emulsions. An example from everyday life is mayonnaise, which is a Pickering water-in-oil emulsion where the vinegar is the dispersed phase, olive oil is the continuous phase, egg yolk is the emulsifier (a surfactant) and small particles of mustard help the stabilization of the emulsion. Pickering managed to create emulsions with up to 60% of oil as the dispersed phase using copper or iron sulphates[33].

In 1923, Finkle wrote the so called Finkle rule, which describes "the correlation between the wettability of particles and their ability to stabilise emulsions"[34]. It also explained the stability of o/w or w/o emulsions depending on the contact angle between the different phases. We call phase inversion to the phenomena that after a certain phase ratio, the dispersed phase become the continuous phase and the continuous phase become the dispersed phase. By tuning the concentration of the different phases, we reach a maximum concentration of the dispersed phase before the phase inversion occurs and change the

dispersed phase into the external phase; this maximum is “strongly dependent on the affinity of the particles for the initial continuous phase”[34]. To evaluate if the particles of emulsifier are stable at the interface between oil and water, we have to determinate its free energy of detachment. This energy is the difference between the surface free energy of the system before and after being absorbed by the interface. As represented in Figure 1.18 the free energy of detachment from the interface toward the water can be calculated as follow (1):

$$\Delta G_{detach} = \gamma_{ow}A^{(2)}_{ow} + \gamma_{pw}A^{(2)}_{pw} - (\gamma_{ow}A^{(1)}_{ow} + \gamma_{pw}A^{(1)}_{pw} + \gamma_{po}A^{(1)}_{po}) \quad (1)$$

Where the γ_{po}, γ_{pw}, and γ_{ow} are the particle-oil, particle-water and oil–water interfacial tensions, respectively.

We can see then, knowing Young's equation, that the contact angle of the particle with each liquid will impact the value of the free energy of detachment. Considering small size and spherical particles (radius R) and a chemically smooth and homogeneous surface, we can obtain from equation (1) the following equation of the free energy of attachment of the particle to the surface ($-\Delta G_{detach}$):

$$\Delta G_{attach} = -\pi R^2 \gamma_{ow}(1 - |\cos(\theta)|)^2 \quad (2)$$

The value obtain via the equation (2) is negative for all the contact angles, which mean that the particles will accumulate at the interface. Like so, Pickering emulsions are very stable emulsion [34].

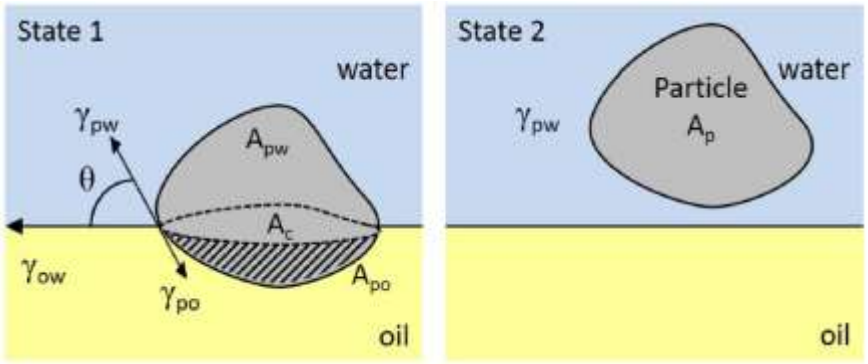

Figure 1.18*: Schematic representation of a solid particle, absorbed in the emulsion interface (state 1) and in the water (state 2).*[34]

Pickering stabilised emulsion polymerisations have been already used to produce nanofoams[31,35–38]. The possibility to stabilise an emulsion up to 70% internal phase (dispersed phase) compared to the external phase without undergoing a phase inversion has been shown by Blaker and Lee [37], using hydrophobized bacterial nanocellulose. Using such a template to realise a poly-Pickering-M/HIPEs (Medium/High Internal Phase Emulsions) [39] could help us getting closer to the 20% solid fraction of cork. Figure 1.19 illustrate a SEM image of the acrylated epoxidized soybean oil (AESO) foam obtained using this method.

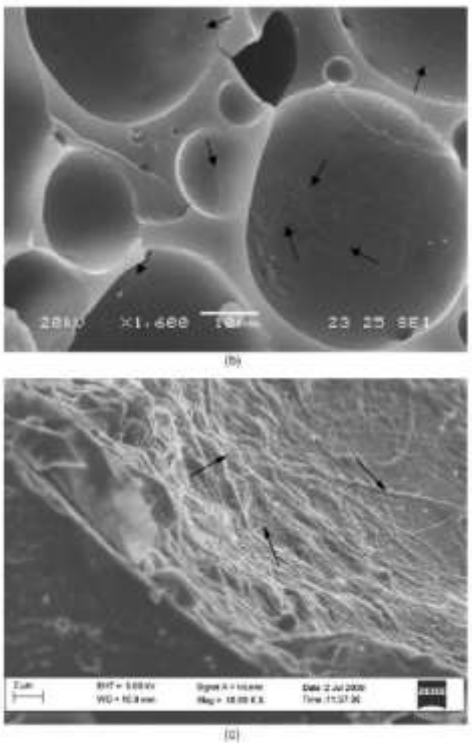

Figure 1.19*: SEM images of the AESO foam obtained by Blaker and Lee* [37]**.**

More recently, in 2014, Tasset *et al.* [40] managed to produce a promising cellular foam "prepared by freeze-drying oil-in-water emulsions stabilized with cellulose nanocrystals"[40]. Figure 1.20 show the SEM picture of these cellular AESO foam obtained in this study. They also showed that the size of the cells can be controlled by the concentration of the oil and the thickness of the wall by the concentration of CNCs.

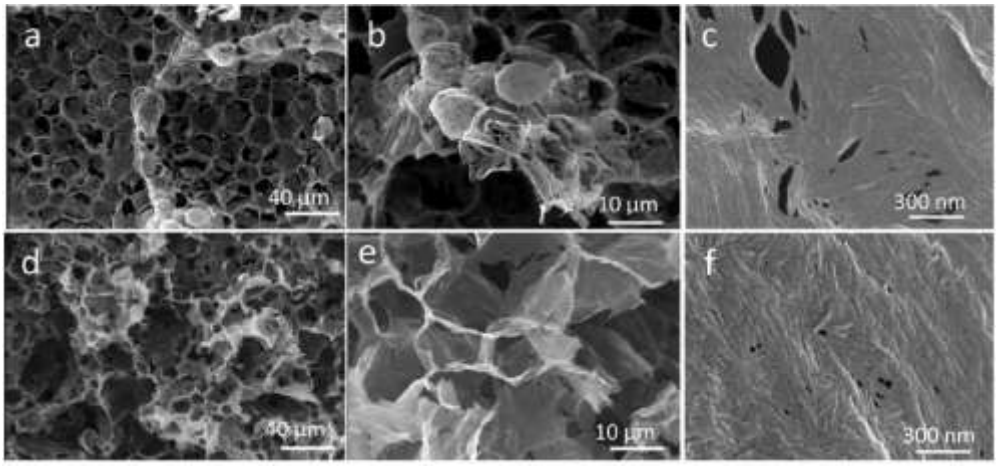

Figure 1.20*: SEM images of cellular foams made of CNCs alone at two concentrations, (a–c) 5 g.L^{-1} and (d–f) 10 g.L^{-1}.*[40]

Inspired by these two studies, and by the need of environmental friendly methods to prepare biomaterials, this study mimics the microstructure and chemical composition of cork tissue by Pickering emulsion approaches using bio-based raw materials in order to produce innovative materials.

2 Experimental part

The following section describes in detail the materials and methods used throughout this study. Firstly the reactants and other chemicals are listed; followed by the comprehensive description of the procedures adopted. Finally, the techniques used for the analysis of the samples are described.

2.1 Materials and reagents

The cellulose substrates used in this study were from two distinct natures, namely: *i)* bacterial cellulose (BC) (three-dimensional network of nano and microfibrils with 10-200 nm width), in the form of wet membranes, produced at our laboratory using the *Gluconoacetobacter sacchari* bacterial strain[41,42] and following established culture procedures[43]; *ii)* microcrystalline cellulose (MCC), under the trade name Avicel PH-101 (3–5 % moisture content), purchased from Fluka.

For the acetylation, the reagents used are: acetic acid anhydride from Chem-Lab (99% - 100% pure) and sulfuric acid from Acros Organics (solution in water, 96% pure).

The monomer used, acrylated epoxidized soybean oil (AESO, containing 4000 ppm of monomethyl ether hydroquinone as inhibitor), divinylbenzene with an 80% mixture of isomers, namely 2-methoxy-4-vinylphenol (DVB, >98%), and 4-acetoxystyrene (>96%) were purchased from Sigma Aldrich-Chemicals Corp.

The photo-initiators adopted to carried out the UV photo-polymerisation reactions, 2-hydroxy-2-methyl-1-phenyl-propan-1-one (Irgacure 1173, old Darocur 1173), 2,2-di-methoxy-1,2-diphenylethan-1-one (Irgacure 651) and 1-hydroxy-cyclohexyl-phenyl-ketone (Irgacure 184), were all purchased from BASF.

All the solvents employed were analytically pure and all other reagents were used as received.

2.2 Methodology

2.2.1 Acetylation of BC

Prior to the acetylation reaction, BC fibres were disintegrated and solvent exchanged from water to ethanol. Briefly, the BC fibres were disintegrated using an Ultra-Turrax equipment at 11 000 rpm, for 1 hour, as illustrated in Scheme 2-1. Afterwards, the BC dispersing solvent was exchanged, by centrifugation, from water to ethanol, and then from ethanol to acetone, using a centrifuge Rotofix 32A and a Pselecta mixta, at 4 500 rpm, during 15 minutes. For each solvent the centrifugation step was repeated five times. The BC was then pressed and filtrated in order to remove the solvent in excess.

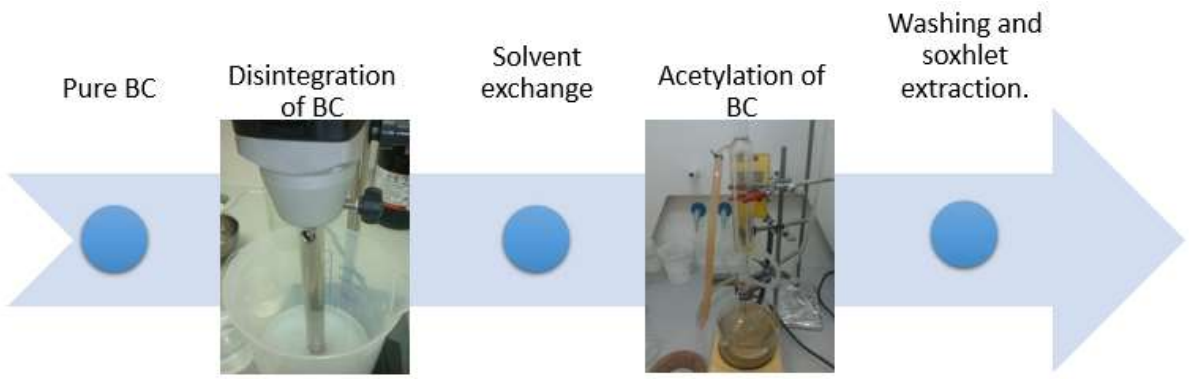

Scheme 2-1: Scheme of the acetylation process.

The BC acetylation was carried out, following a procedure described by Gandini et al.[44]. Approximately 300 mL of acetic acid anhydride and 1 mL of H_2SO_4 were added to 20 g of BC, the mixture was heated at 30 °C, during 4 hours, under a N_2 atmosphere. Then, the reaction mixture was stirred with an excess of water and the acetylated BC (Ac-BC) fibres isolated and washed sequentially with cold acetone, ethanol, water, and finally again with ethanol.

Subsequently, aiming at removing any residual trace of acetic anhydride and/or other impurities, the fibres were Soxhlet extracted with ethanol, during 12 hours. The Ac-BC fibres were dispersed in water and they were ready for the emulsion preparation acting as a stabiliser.

2.2.2 Pickering emulsion polymerisation of AESO

2.2.2.1 Water-in-AESO Pickering emulsions

The water-in-AESO emulsions were prepared following an adapted procedure described by Blaker and Lee[37]. Typically, they were performed in a Falcon tube (50 mL) using approximately 10 mL of AESO and 10 ml of water containing 0.5 wt% of Ac-BC. The mixture was heated at 80°C, for 30 minutes, and promptly homogenized by hand shaking during 1 minute. This procedure was repeated every 12 hours, for 7 days. The ensuing product was a stable emulsion after 3 days (Figure 2.1) as will be explained, in detail, in the next section (3. Results and discussion).

Figure 2.1: Stable water-in-AESO (above the red line) emulsion and ejected AESO (under the red line).

To polymerise the AESO with the MCC particles inside the matrix, the same procedure was used, but after adding the water, 1.1 g of MCC was added to the mixture. Then the procedure was carried out in the same way as the previous preparation.

2.2.2.2 Water-in-AESO/cyclohexane Pickering emulsions

Water-in-AESO/cyclohexane emulsions were also prepared following the same procedure described by Blaker and Lee[37]. Typically, these emulsions were prepared in a Falcon tube (50 mL) using approximately 5 mL of AESO, 5 mL of cyclohexane and 10 ml of water containing 0.5 wt% of Ac-BC. First the 5 mL AESO and the 5mL of cyclohexane were

homogenised using an ultrasound bath, for 1 minute. Then, the water and Ac-BC was added to the mixture, promptly homogenised by hand shaking, for 1 minute and allowed to rest for 12 hours, at about 4 °C. Finally, the mixture was re-agitated. The ensuing product was a stable emulsion after 3 days of resting, as illustrated in the picture of Figure 2.2.

Figure 2.2: Stable water-in-AESO/cyclohexane emulsion (under the red line) and ejected AESO/cyclohexane (over the red line)

2.2.2.3 Photo-polymerisation of water-in-AESO emulsions.

Typically, the UV-photoinitiator Irgacur 1173 (0.4 wt% relatively to AESO) was added to the water-in-AESO stable emulsions (4 days), the mixture was shaken by hand, and heated at 80 °C (capped and protected from light) until a stable emulsion volume (around 15 mL) was reached. Samples were then irradiated during 6 hours with UV light, using a mercury lamp (100 W and >280 nm), to photopolymerise the AESO phase. The ensuing foams were removed from the Falcon tube and dried, during 24h at 50 °C. Figure 2.3 shows an illustrative picture of an AESO-foam obtained by this process.

Figure 2.3: Transversal cut of an AESO foam produced by UV photopolymerisation of Pickering emulsion stabilised with cellulose nanofibers.

2.2.2.4 Photo-polymerisation of water-in-AESO/cyclohexane emulsions.

The water-in-AESO/cyclohexane emulsions were polymerised using a similar process. The UV-photoinitiator Irgacur 1173 (0.4 wt% relatively to AESO) was added to the water-in-AESO/cyclohexane stable emulsions (4 days), shaken by hand, and left in the refrigerator (capped and protected from light) until a stable emulsion volume (around 15 mL) was reached. The ejected oil phase (5 mL) was removed, then the samples were irradiated during 6 hours with UV light, using a mercury lamp (100 W and >280 nm), to photopolymerise the AESO phase. The ensuing foams were removed from the Falcon tube and dried, during 24h, at 50 °C. Figure 2.4 shows an illustrative picture of an AESO-foam obtained by this process.

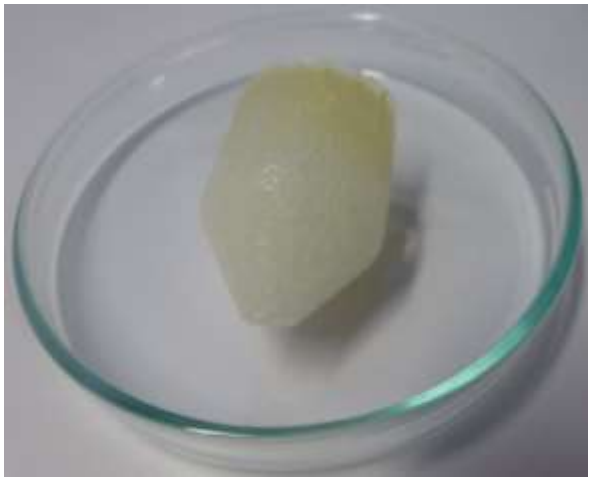

Figure 2.4: AESO foam produced by UV photopolymerisation of water-in-AESO/cyclohexane Pickering emulsion stabilised with cellulose nanofibers.

2.2.3 Photo-polymerisation of aromatic monomers

Divinyl benzene, 2-methoxy-4-vinylphenol and acetoxy-styrene monomers were photo-polymerised according to the following process: approximately 0,4 g of each monomers were mixed with 0,4 wt% of photo-initiator (Irgacur 184, 651, 1173). The mixture was then deposited on a lamella, and exposed to a UV radiation (11 W, 280 nm) during 6 to 8 hours to photopolymerise the monomer. The obtained films were the washed with chloroform to remove any residues of monomer and/or initiator, and dried.

2.3 Characterisation

The obtained materials were characterised using several techniques including Attenuated Total Reflection Fourier Transform Infrared spectroscopy (ATR FTIR), Thermogravimetry Analysis (TGA), Dynamic Mechanical Thermal Analysis (DMTA), optic microscopy and Scanning Electron Microscopy (SEM).

2.3.1 Attenuated Total Reflection Fourier Transform Infrared Spectroscopy

The ATR FTIR spectra were acquired using a Paragon 1000 Perkin-Elmer FTIR spectrophotometer equipped with a single horizontal Golden Gate ATR cell. The spectra were recorded at a resolution of 4 cm^{-1}, after 64 scans with a range of 1 cm^{-1}.

2.3.2 Thermogravimetric Analysis

TGA analyses were carried out with a SETSYS Setaram TGA analyser equipped with a aluminum cell. Typically, samples (~17 mg) were heated at a constant rate of 10 $^{o}C.min^{-1}$, from 25 °C to 800 °C, under a nitrogen flow of 20 $ml.min^{-1}$.

2.3.3 Dynamic Mechanical Thermal Analysis

DMTA measurements of thick specimens (1 x 1 x 0.6 cm^3) were carried out with Tritec 2000 DMTA Triton equipment operating in the compression mode. Tests were performed at 1 and 10 Hz, and the temperature was varied from -50 to 200 °C at 2 °C min^{-1}. Each measurement was repeated up to three times.

2.3.4 Optical microscopy

The optical microscope images were captured with an IDS UI124DML numerical camera mounted on an Olympus Microscope BX51, with options of magnification as follow: ocular x10 and objectives x5, x10 and x20.

2.3.5 Scanning Electron Microscopy

SEM images of the cross-section of foam specimens were acquired using a field emission gun-SEM Hitachi SU70 microscope operated at 15 kV. Samples were deposited on a sample holder. Before observation, the samples were coated twice with evaporated carbon. The magnifications used to capture the pictures were x60, x130, x1500, x2500 and x15000.

3 Results and discussion

Cork is an interesting material with unique properties, as have been emphasised throughout this Thesis and in particular in Chapter 1. Inspired by cork unique features, in the present study, novel cellular foams based essentially on soybean oil and cellulose were developed. These foams were prepared by Pickering emulsion polymerisation of acrylated epoxidised soybean oil (Figure 3.1) selected as the continuous oil phase, because it is composed of fatty acids linked with glycerol, closely resembling the chemical composition of cork's suberin. The dispersed phase was water. Additionally, we have selected Ac-BC nanofibrils for stabilising the Pickering emulsion in order to mimic the cork composition. Moreover, the nanofibers were embedded inside the foam, also resembling the architecture of cork. Hence, the ensuing emulsions were w/o.

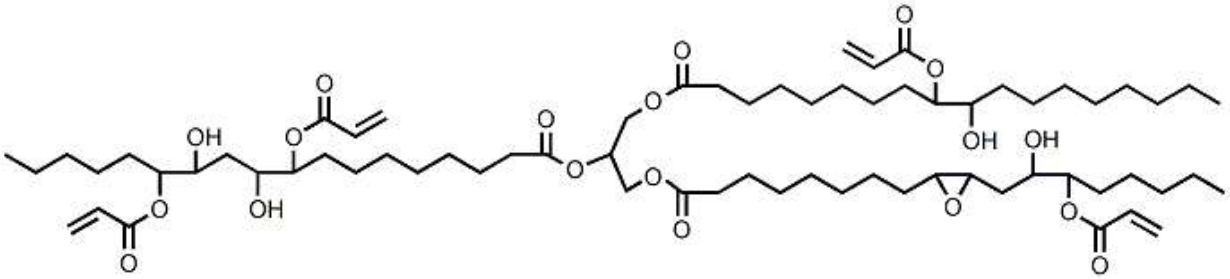

Figure 3.1: Structure of acrylated epoxidised soybean oil (AESO)[45].

The stability of the emulsion and the water/oil ratio were assessed by visual inspection and optical microscopy. At each step of biomaterials preparation, the products of the reaction were extensively characterised by ATR FTIR and SEM. Additionally, The ensuing foams were characterised with SEM, TGA and DMTA.

The following sections present the main results and discussions of acetylation of bacterial cellulose nanofibers (section *3.1*), stabilisation of Pickering emulsions (section *3.2*), the UV photopolymerisation of AESO (section *3.3*) and finally the characterisation of the ensuing products (section *3.4*). All the experimental details related with the present

chapter are summarised in Chapter 2.

3.1 Acetylation of bacterial cellulose fibres

After purification and hydrophobisation of the cellulose nanofibrils, we can use them as a stabilizer of the Pickering emulsion. The nanofibrils will assemble themselves in a cellular template which will be the basis of the emulsion polymerisation of the AESO.

After biosynthesis, bacterial cellulose fibrils are naturally hydrophilic. In order to be used as stabilisers for w/o Pickering emulsions, the contact angle BC/water, also called advancing contact angle, had to be increased[37], to do so they were hydrophobised by acetylation of the hydroxyl groups. The acetylation reaction was perform by adapting acetylation reactions conditions from litterature[37,44]. However, oppositely to the some acetylation procedures described in literature, such as the one by Blacker *et al.* [37], the one we have adopted is more environmentally friendly, avoiding accordingly the massive use of toxic solvents, pyridine or p-toluenesulfonyl chloride and hard reaction conditions. The procedure adopted here was carried out using only acetic anhydride and sulphuric acid. The acetylation reaction is schematically represented in Scheme 3-1.

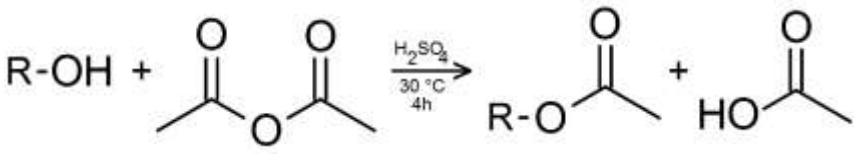

Scheme 3-1: ***Acetylation reaction.***

The success of this reaction was confirmed by ATR FTIR spectroscopy, as clearly shown in Figure 3.2, by the appearance of a new characteristic band near 1735 cm^{-1}, typically ascribed to the stretching mode of the carbonyl ester groups ($\nu_{C=O}$)[46]. Besides the appearance of this band, a significant reduction of the O-H stretching modes (at 3342 cm^{-1}, respectively) also confirmed the acetylation reaction occurred and moreover pointed out for an extensive acetylation of BC fibres, which most probably has occurred not only at the surface but also at the bulk. The impact of the degree of acetylation on the emulsion

stability and hence on foams morphology and related mechanical properties would be of upmost interest to be apprehended in further studies.

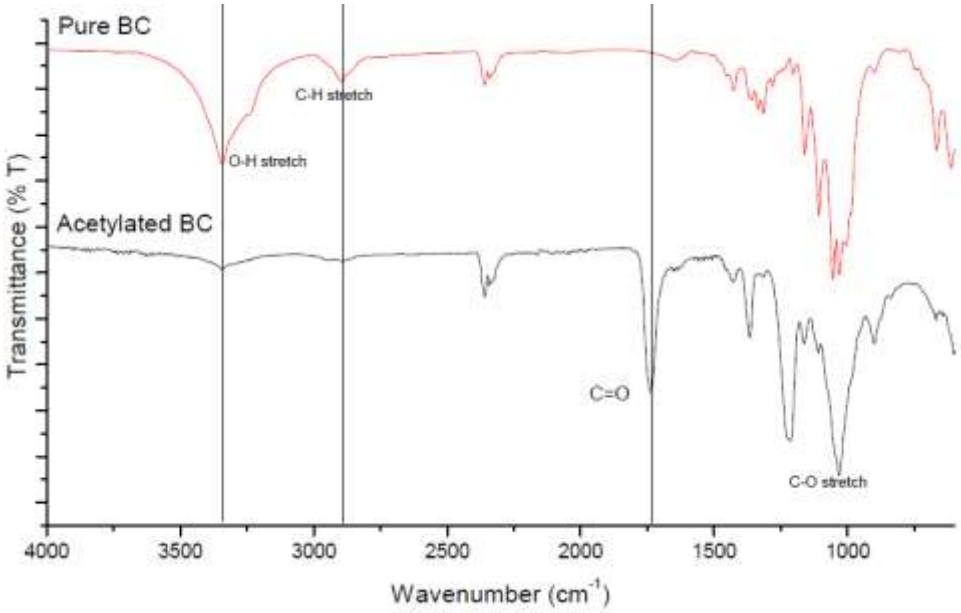

Figure 3.2: FTIR spectra of BC before and after acetylation.

The hydrophobic nature of the Ac-BC fibres was evident by their low affinity to acetone, ethanol and especially water used during washing and solvent exchanges. In the work of Blaker *et al.*[37], they reported an increased contact angle of 64° (from 11° to 75°) from neat BC to acetylated BC. The contact angle of the Ac-BC films were measured at roughly 77°, which confirm the hydrophobisation of the BC.

3.2 Preparation of Pickering emulsions

In order to create a cellular material, the AESO monomers must be positioned at the interface of the Pickering emulsion embedding Ac-BC fibres, hence the emulsions will be water-in-oil (w/o) emulsions, using Ac-BC as stabiliser. Note that, although AESO was already used in the preparation of foam materials it has never been introduced directly in the emulsions before, instead AESO was added by long-time oil exchange procedures.

The emulsions stability is of upmost importance for the ensuing foam properties, especially

its morphology and related mechanical performance. Therefore, prior to polymerisation reactions, we have studied the stability of water-in-AESO emulsions (Figure 3.3). The emulsions stability is obviously strongly related with the selected oil, and the ratio oil/water; besides the properties of the Ac-BC.

We have studied the water-in-AESO emulsion stability, during 10 days, using optical microscopy; and also by visual inspection and measuring the volume of ejected oil. According to literature it can take between 3 days[37] to 7 days[47] to obtain a stable emulsion after mixing the soybean oil, water and Ac-BC and shaking this mixture for 1 minute by hand, every 12 hours. Before shaking by hand, the volume of the emulsion and the volume of ejected oil were measured and when the volume stayed unchanged for several days, the emulsion was considered stable. Table 3-1 summarises the various emulsions prepared in order to study the emulsion stability.

Table 3-1: Experimental data related with the study of the emulsions stability.

	Compounds feed						**Ensuing Emulsion**
Emulsion	V_{water} /mL	V_{AESO} /mL	$V_{Soybean\ oil}$ /mL	w/o[a]	Ac-BC (wt% in water)[b]	Tube diameter /cm	**% of internal phase**
E1	20	0	20	0.5	0.2	2.7	50%
E2	24	0	16	0.67	0.2	2.7	52%
E3	8	8	0	0.5	0.5	2.7	63%
E4	12	8	0	0.67	0.5	4.7	67%
E5	10	10	0	0.5	0.5	2.7	65%
E6	10	10	0	0.5	0.5	4.7	50%

[a] Volume ratio between the oil phase and the water phase.

[b] Mass of Ac-BC added into the water phase, in wt% compared to the oil phase.

In general, only after 3 days a stable water-in-AESO Pickering emulsion, prepared with a feed ratio of water/AESO equal to 50/50 (V/V %) and 0.5 wt% of Ac-BC (E1, E3 and E5), was obtained. Figure 3.3 presents the average values of the tests done on the water-in-AESO emulsions beside a picture of the stabilised emulsion in the 45 mL Falcon tube.

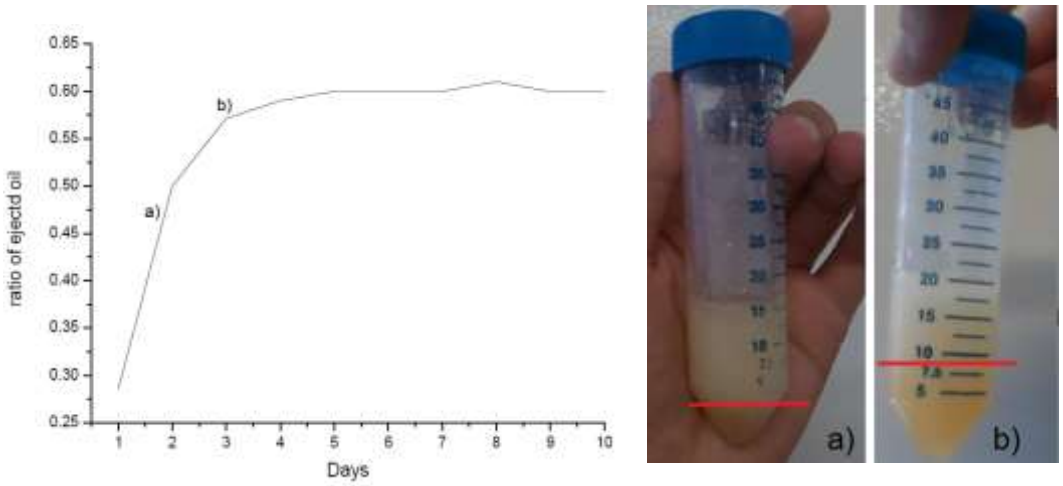

Figure 3.3 : Evolution of the ejected oil ratio as a function of the days of shaking. On the right are two pictures of the Falcon tubes containing the emulsion E3 after one day (a) and the emulsion E5 after three days of preparation (b).

As we can see in Table 3-1 and Figure 3.3, the ejected oil ratio was about 60%, thus the remaining emulsion has around 60% internal phase. We can conclude that we have indeed prepared a High Internal Phase Emulsions (HIPEs)[48]. This condition is primordial, as cork material has a solid fraction of 10%, this HIPEs can produce a 30 to 40% solid fraction foam.

The optical microscopy imaging (Figure 3.4) allowed confirming the identity of each phase. Typical microscopy images of Figure 3.4 of the upper phase (usually called emulsion phase, visible in Figure 3.3) confirmed on the one hand that we have the characteristic appearance of a HIPE with micro-sized water droplets, and on the other hand the bottom phase (ejected oil phase) have a more homogeneous with only rare and small water and air droplets.

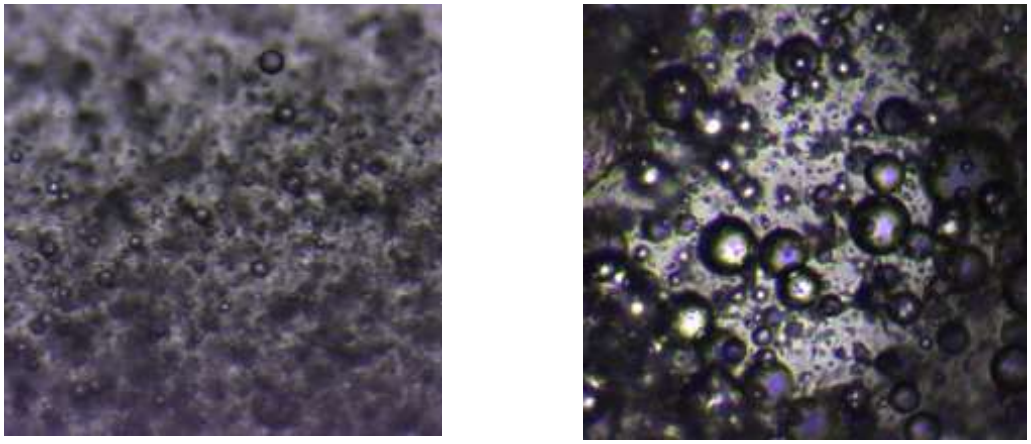

Figure 3.4: Optical microscopy images at 20 times magnification of ejected oil phase (left) and the emulsion phase (right) of the control sample E5 (50/50 water-in-AESO emulsion).

Additionally, in order to have a higher surface area on the top of the reaction tube and hence, in the polymerisation step, to directly irradiate the sample in a higher surface area and, thus, to promote a more rapid and higher extension of polymerisation, stabilisation of emulsion in a larger tube (plastic cup with 150 mL) was tested. The emulsion E6, prepared in a 150 mL plastic tube, was compared to sample E5, prepared in a 45 mL Falcon tube. However, stabilisation of this emulsion was not possible with such a wide surface of contact between the emulsion and the air. Non-homogeneous water phases were obtained with a few much bigger water droplets in the emulsion.

Additionally, we have also prepared water-in-soybean oil emulsions (E1 and E2) following exactly the procedure described by Bismark et al.[37] (Table 3-1). However, this procedure involved a laborious step consisting of a phase-exchange from unmodified soybean oil to AESO. Another aspect of upmost importance is that these emulsions had a lower internal phase ratio (c.a. 50%) which qualified the emulsions as medium internal phase emulsions (MIPEs),[48] oppositely to the water-in-AESO (E3-6).

The E5 emulsion had a concentration of cellulose of around 1% of BC in the final product. Comparing this value with the 20% of cellulose in cork material, it is obvious we

had to find a way to increase the cellulose concentration in the final product. Table 3-2 provides a comparison of emulsion E5 with the two emulsions prepared in order to increase the proportion of cellulose in the final foam.

Table 3-2: Comparison of E5 with E7 and E8 in order to increase the concentration of cellulose in the foam, the expected cellulose concentration is also represented.

Emulsion	Compounds feed						Ensuing products
	V_{water} /mL	V_{AESO} /mL	$V_{cyclohexane}$ /mL	w/o[a]	Ac-BC (wt % in water)[b]	m_{MCC} /g	% of cellulose expected in the foam
E5	10	10	0	0.5	0.5	0	**0.96%**
E8	10	5	5	0.5	0.5	0	**2%**
E7	10	10	0	0.5	2	1.1	10%

[a] Volume ratio between the oil phase and the water phase.

[b] Mass of Ac-BC added into the water phase, in wt% compared to the oil phase.

To increase the cellulose concentration in the obtained product we mixed the AESO with cyclohexane before preparing the emulsion E8. With an oil phase composed of equal volumes of AESO and cyclohexane, the concentration of cellulose in the final product was doubled, i.e., it reached 2 %. Figure 3.5 presents a picture of the obtained emulsion, showing the ejected oil at the top of the emulsion phase.

This ejected oil was removed before the photo-polymerisation reaction. However, for the water-in-AESO emulsion, removing the oil phase means putting a pipette through the emulsion phase and this procedure was found to destabilise the emulsion. From this observation, it was decided to perform the polymerisation with both phases and to cut out the ejected oil phase afterwards.

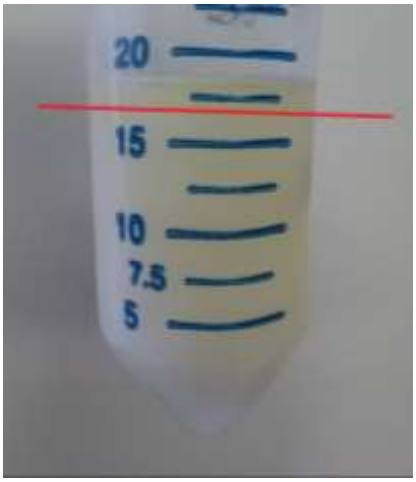

Figure 3.5: Emulsion E8 of water-in-AESO/cyclohexane

This new emulsion using a mixture of AESO and cyclohexane as the oil phase, in order to stabilise a higher internal phase emulsion, besides increasing the concentration of BC in the ensuing foam, also reduced the viscosity of AESO which allowed to simplify the emulsion preparation, avoiding thus the need for heating and also reducing the time needed to have a stable emulsion (around 2 days).

Another strategy was tried (E7) to increase the cellulose content in the obtained foam. We aimed to stabilise the emulsion with as much Ac-BC as it was tried in the literature[37], i.e. 2wt% of the water phase, we added to this mixture the remaining mass of microcrystalline cellulose (MCC) needed to obtain an expected cellulose concentration of 10%. However, we did not managed to create a stable emulsion, the introduction of MCC seems to destabilise the system. The hydrophilic microcrystalline cellulose was probably the cause of this destabilisation.

3.3 Optimisation of UV photopolymerisation of AESO

Once the conditions needed to obtain a stable emulsion were optimised, i.e. 50/50 w/o ratio with 3 days heating for water-in-AESO and 2 days rest for water-in-AESO/cyclohexane, the photopolymerisation reactions were performed. In the following part, we describe and discuss the different foams produced by UV-photoplymerisation, and how from these observations we optimised the photopolymerisation of AESO.

Choosing between two lamp (different powers) and the conditions of polymerisation, four samples were polymerised. The conditions of these experiments are summarised in the Table 3-3.

Table 3-3 : Experimental data related with the four foams produced by UV photopolymerisation and experimental conditions.

Foam	Emulsion	% AESO/ Cyclohexane[a]	Act BC (wt% in water)[b]	Cup diameter	UV Lamp characteristics	Observations
F1	E3	50/0	0.5	2.7	**Hg** 11W λ>280nm	**Inside not polymerised**
F2	E5	50/0	0.5	2.7	**Hg** 100W λ>280nm	All volume polymerised
F3	E8	25/25	0.5	2.7	**Hg** 11W λ>280nm	**Inside not polymerised**
F4	E8	25/25	0.5	2.7	**Hg** 100W λ>280nm	All volume polymerised

[a] Volume ratio of AESO or cyclohexane compared to the total volume of the liquid added (water and oil phases).

[b] Mass of Ac-BC added into the water phase, in wt% compared to the oil phase.

Two mercury (λ>280nm) UV lamps with different powers (11 and 100 W) were used to photo-polymerise AESO monomer into the corresponding AESO polymer[49] (PPAESO). Using the 100W lamp, the ensuing foams (F2 and F4) were efficiently polymerised in all extent of its depth as confirmed by ATR FTIR. Figure 3.6 shows the FTIR spectra of F2's PPAESO of the inside and outside of the foam compared with the one of AESO monomer. The success of the polymerisation was confirmed by the strong decrease in the intensity of the acrylate moiety related bands, the decrease of the C=C bond stretching at 1617–1636 cm^{-1}; as well as the in-plane C-H deformation of $C-H_2$ at 1406 cm^{-1} (i); and at 810 cm^{-1} (ii) and 984 cm^{-1} (iii) the out-of-plane deformation of $C-H_2$[46].

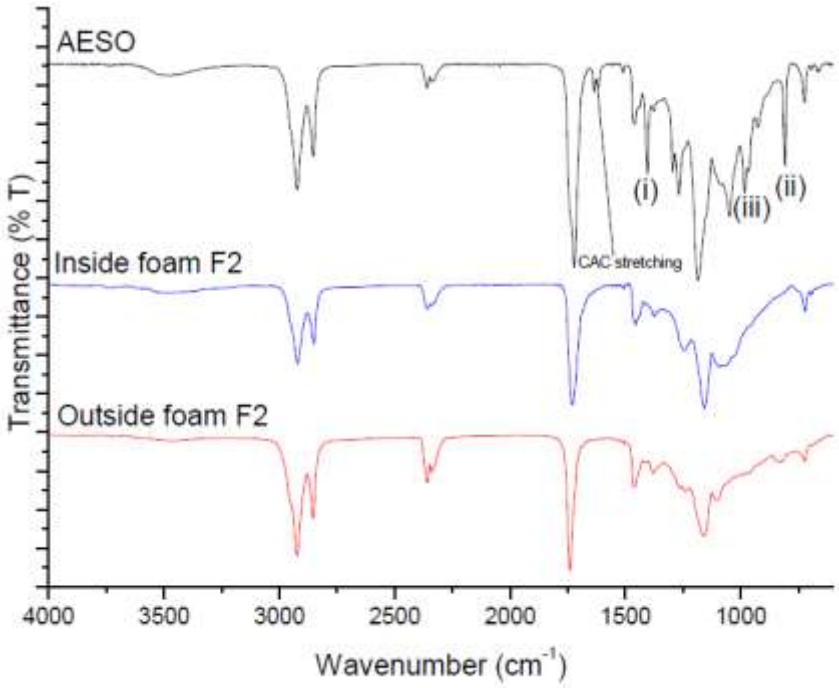

Figure 3.6 : ATR FTIR spectra of AESO monomer and ensuing PPAESO of the F2's outside (left), as well as the ATR FTIR of the inside of the F2 foam (right).

The 11 W UV-lamp been faster and easier to manipulate it was our choice for the first polymerisation reactions: the F1 and F3 foams. However, after the polymerisation it was clear that the middle of the F1 foam was not polymerised. Figure 3.7 shows clearly this problem on the picture of the foam and on the comparison of the FTIR in different part of the foam, where we can see that the double bound C=C stretching band does not disappear in the FTIR spectra of the inside of the foam compared to the spectra of the AESO monomer.

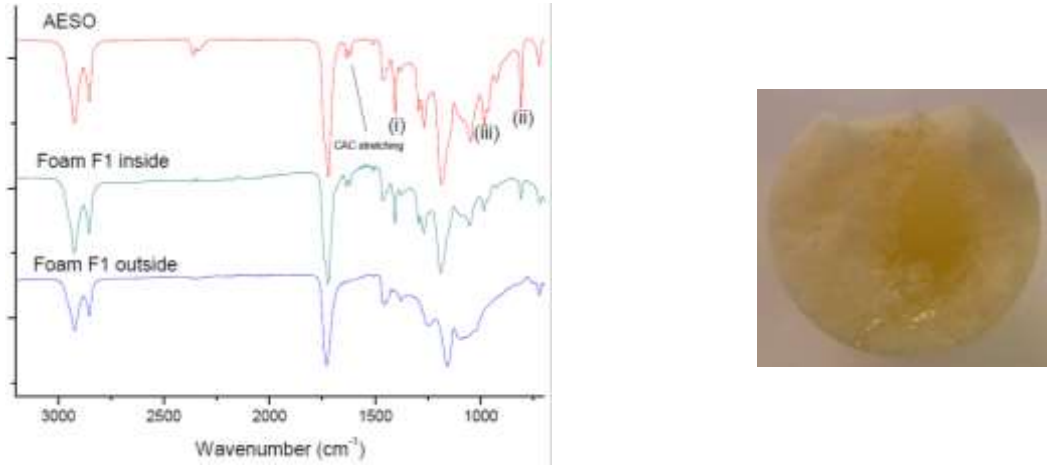

Figure 3.7 : FTIR spectra of the inside and outside parts of the F1 foam compared to the AESO monomer spectra (left). Picture of the F1 foam (right).

The polymerisation of the E8 emulsion was also firstly carried out with the 11 W lamp first (foam F3). As we can see on Figure 3.8, the polymerisation of the F3 foam was not totally successful; we can see that the inside of the sample is not well polymerised as expected from previous results. But the material obtained is cellular and the cyclohexane does not evaporate under the heat of the lamp quickly enough to destabilise the emulsion. And we can also see on the Figure 3.8 the full polymerisation of the F4 foam using a lamp with a higher power (100 W).

Figure 3.8: Picture of F3 (left) after a longitudinal opening compared with the transversal cut of F4 (right).

3.4 Characterisation of the ensuing foams

This section is focused on the analysis of foams (F2 and F4) obtained after

optimisation of the procedures previously described. Both foams were characterised using SEM imaging and thermal stability was evaluated by TGA. Dynamic Mechanical Thermal Analysis (DMTA) was also performed to characterise the thermo-mechanical properties of the foam. These properties are comparable to cork material and improved as we bring the composition of the foam closer to the one of the later.

3.4.1 SEM images

In Figure 3.9 two typical SEM images of F2 and F4 foams, at x60 and x30 magnification, respectively, provide a general overview of their morphology. The SEM images were analysed using an image analysis software, the results of the cell count and measurement are shown in the table 3.4. The two foams have both the internal phase ratio of a HIPE. However, the cell size of the foams varies from 410 µm for F2 to the double (881 µm) for F4.

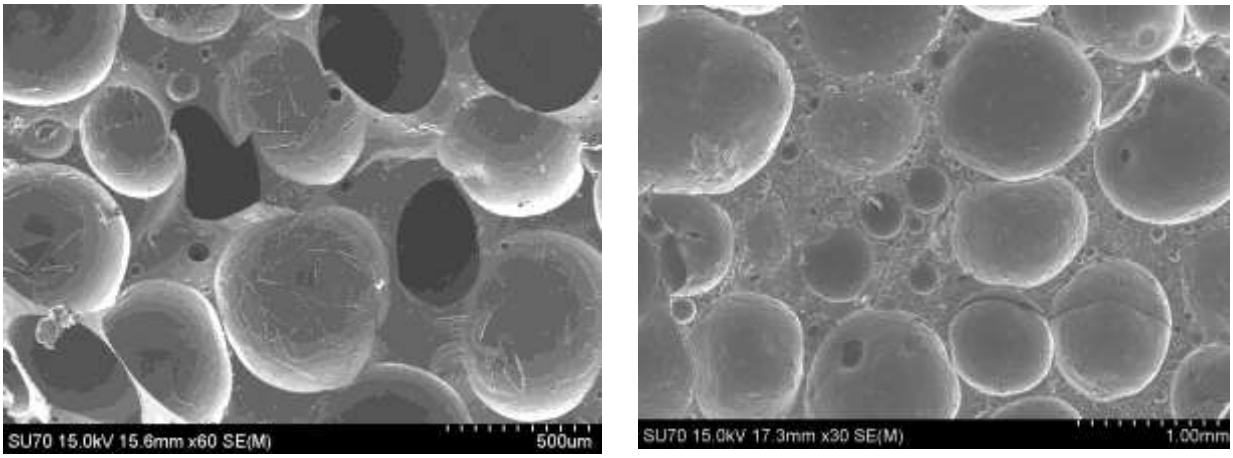

Figure 3.9: SEM images of foams F2 (left) and F4 (right), at x60 and x30 magnification respectively

Table 3-4: SEM image analysis results

Foams	Main cells average size (µm)	Standard variation (µm)	% of standard variation
F2	410.7	198.7	0.48
F4	881.1	399.5	0.79

Note that the homogeneity of the cell size also varies, the continuous part of the F2

foam is smoother and with less porosity than in F4 foam. Figure 3.10 represents a close-up of the continuous phase of each foams. This characteristic is also shown by the standard variation % of the table 3-4. This difference is probably due to the evaporation of the cyclohexane from the oil phase after polymerisation of the AESO, we can also see this phenomenon on the side of the bigger cells.

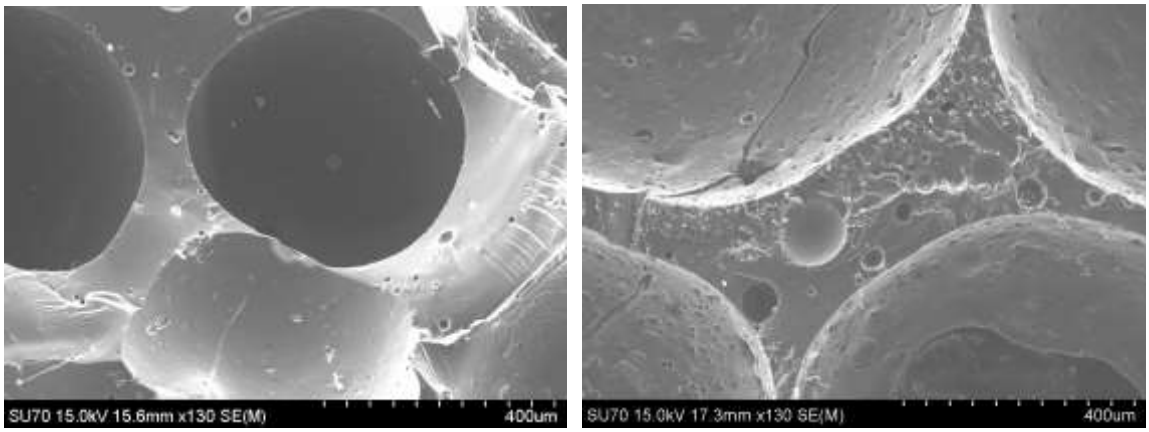

Figure 3.10: x130 magnification close-up of the continuous phase of the foams F2 and F4

With a higher magnification on the side of a cell, we can see the embedding of the cellulose fibres in the matrix of the PPAESO. Figure 3.11 shows the magnification of the cell's wall compared to SEM picture of modified bacterial cellulose x15000, on this pictures we can see the modified cellulose fibres showed by the black arrows.

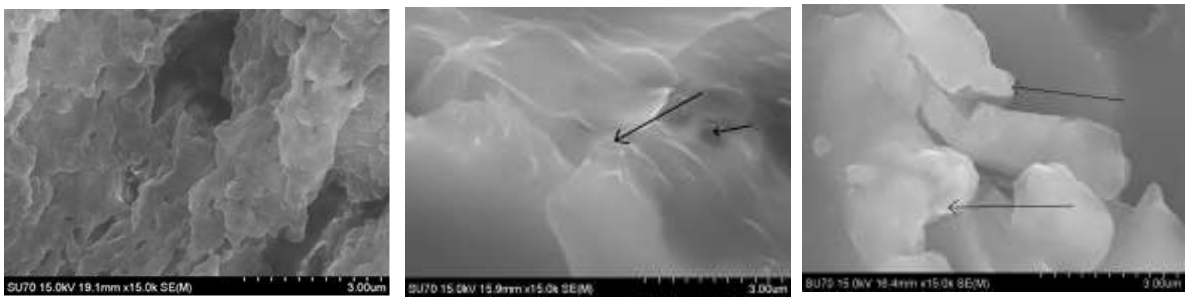

Figure 3.11: SEM images at a magnification of x15000 of the Ac-BC (left), of the foam F2 (centre) and the foam F4 (right) where arrows show the Ac-BC.

3.4.2 Thermogravimetric Analysis

Thermogravimetric analysis was used to study the thermal stability of the nanocomposite foams and of the corresponding individual components.

Figure 3.12 shows the TGA curves of the bio-foams F2 and F4 as well as the TGA of Ac-BC and AESO monomer. Results revealed that this foam was thermally stable up to 260 °C (at 5 % weight). The foam's thermogram showed a three step weight loss profile displaying decompositions due to both modified BC and the AESO polymer, the main peaks of this curves are listed in the Table 3-5. Starting to degrade at around 130 ºC and reached their first maximum decomposition between 163-168 ºC (at 3% weight loss), probably due to the water release. The second degradation step of the nanocomposite corresponded to the degradation of the AESO and began at 253 °C with a maximum at 381-384 °C as well as the last observed decomposition step have a maximum at 416-420 °C, followed by a slower complete volatilization ending near 500 °C. The shift of the TGA peak at 380 °C can be explained by the presence of the Ac-BC peak at 361 °C.

Table 3-5: Maximum degradation temperatures ($T_{d,max}$) of AESO and F2 and F4.

Samples	$T_{d,max}$ (/°C)		
AESO		388	420
Ac-BC		361	
F2	168	384	416
F4	163	381	416

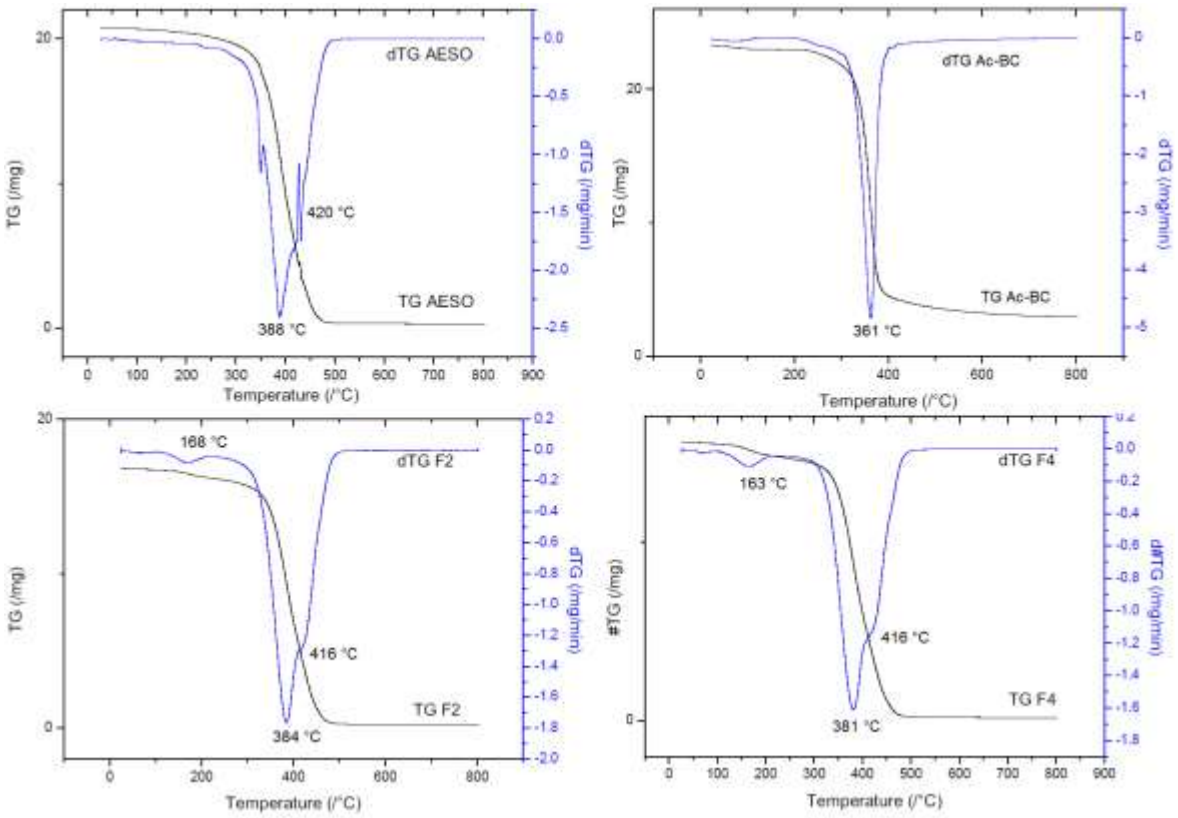

Figure 3.12: Thermogravimetric trace of the foam F2, showing a three step degradation profile

In comparison with cork material[50], the first degradation around 170°C for 3.85% weight loss was also measured by A. Mir and his colleagues[50]. Also, the degradation around 380°C, correspond to the suberin degradation measured by Gandini et all[13], as well as the 80% volatilization at 470°C (427°C in our case).

3.4.3 Dynamic Mechanical Thermal Analysis

DMTA analysis was performed in compression mode to investigate the mechanical properties of the new bio-foams. Figure 3.13 displays the storage modulus vs temperature and the tan δ vs temperature curves (E' vs T and tan δ vs. T) of F2 and F4 foams. We can see that the storage modulus of both foams decrease with increasing temperature due to the softening of the material. This inflection of the E' vs T plots is related with the occurrence of a relaxation process. The tan δ vs. T curves of both foams show two transitions, a first smaller one at sub-ambient temperatures and a second broader transition at higher

temperatures. Similar DMTA curve profiles (tan δ vs. T) were also described in literature for cork material[51,52].

The tan δ vs T curve of F2 foam displays the second transition at a maximum temperature of approximately 30 °C (*f* = 1 Hz), while in the case of F4 foam, it was found at much higher values, ca 60 °C (f = 1 Hz), probably due to the highest amount of Ac-BC in the latter foam. Furthermore, this transition is frequency dependent (roughly 12 ºC difference), and hence is ascribed to the glass transition temperature.

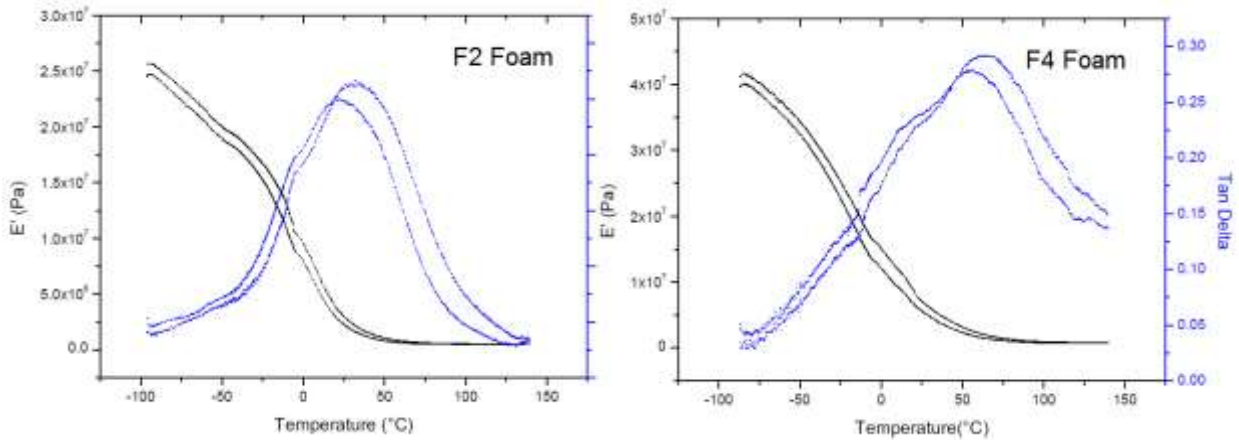

Figure 3.13: Storage modulus and tan δ in function of the temperature of foams F2 (Left) and F4 (Right) obtained by DMTA analysis in compression mode.

The shift of the second transition temperature (from 30 °C to 62 °C) could be explained by the increase in the crosslinking which is associated with the density decrease of AESO when mixed with cyclohexane. The full interpretation of DMTA behaviour still, however, needs further investigation.

Conclusion

For such an ancient material as cork is, the multiple ways of use and applications of cork are impressive. However, only in the last decades, with the increase interest on innovative bio-based materials for different technologies, cork has been used for other applications rather than bottle stoppers. Its properties, like hydrophobicity, thermal and acoustic isolation, high energy absorption, high friction among others, are due to cork microstructure and chemical architecture and these were a source of inspiration for the herein presented study.

Indeed, by mimicking this rare microstructure and chemical composition, bio-based high performance materials were developed, specifically in this study we used nanocellulose fibrils as stabiliser of a water in an acrylated soybean oil Pickering emulsion (w/o).

Novel bio-based foams, entirely based on renewable resources, were successfully produced by environment friendly approaches based on photo-polymerising water-in-AESO emulsions. The cellular-like microstructure of these foams was confirmed with SEM imaging and it was found that cells had an average diameter ranging from 410 to 800 µm.

Moreover, it was found that this microstructure, especially the pore size and density can be simply tuned by changing the AESO/water ratio. The maximum decomposition temperature, determined by TGA, of the ensuing foams were found to be up to 427 ^{o}C. The mechanical properties of the foams were studied by DMTA, and the glass transition value was found to be between 30-60 ^{o}C, most probably associated with the amount of Ac-BC incorporated.

Finally, a few words to highlight that the present study, carried out during this thesis, above all contributes to the development of novel biomaterials inspired by nature, following the pertinent need to develop sustainable materials by eco-friendly approaches. Moreover, after this thesis, some future investigation directions were opened, representing new and stimulating challenges. In further studies it would be interesting to compare the impact of the degree of acetylation of BC on the stability of the emulsions and on porosity.

Also, another challenge is the preparation of bio-foams, incorporating lignin-like monomers, such as DVB, which will have an impact in the foam properties, especially their thermal behaviour.

Annexe 1 :

UV-Polymerisation of aromatic monomers:

In order to closely mimic cork the novel biomaterial, should have in its chemical composition suberin-like monomers and cellulose, as the previously described foams, besides possessing an aromatic fraction, usually associated with lignin. Indeed, lignin has a primer importance in the structure and composition of cork material as described above in section 1.1.4.2 in more detail. In this study several aromatic-monomers were considered to mimic lignin-monomers, namely, 2-methoxy-4-vinylphenol, acetoxystyrene and divinylbezene (DVB) (Scheme 1). Each of these monomers has an aromatic part and a vinyl group which allowed their radical polymerisation. DVB is also interesting considering the possibility of crosslinking while polymerising.

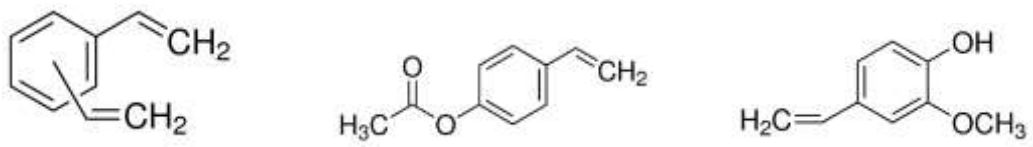

Scheme 1: From left to right: divinylbezene (DVB), acetoxystyrene and 2-methoxy-4-vinylphenol.

The polymerisation of DVB was carried out with three different initiators. The PDVB spectrums are represented on the Figure 1, the characteristic peaks of PDVB can be observed. The absorption peaks at 700-750 cm^{-1} are benzene ring deformation vibrations[53]; the absorption peaks at 1500, 1600 cm^{-1} are associated with benzene ring C = C stretching vibration[53] and the aliphatic C-H stretching vibration is observed at 2920 cm^{-1} whereas 3030 cm^{-1} showed the characteristic peaks of aromatic C-H stretching vibration[53].

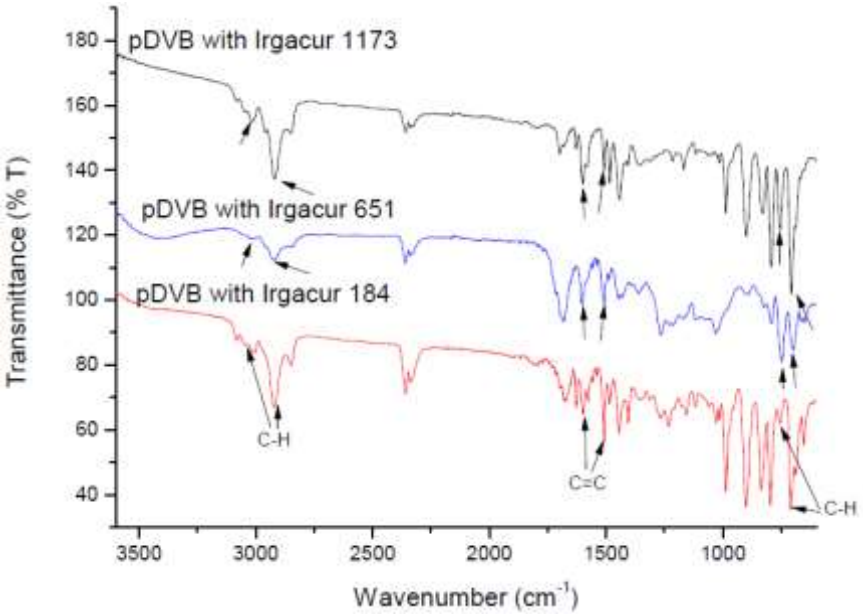

Figure 1: PDVB spectra UV-polymerised with different initiators

References:

1. H. Pereira. *Cork: Biology, Production and uses*. Elsevier B.V.: Germany, 2007.

2. J. Gul, S. M. Effect of Cork Loading on Mechanical and Thermal Properties of Silica-Ethylene-Propylene-Diene Monomer Composite. *Key Eng. Mater.* **510-511,** 277–283 (2012).

3. APCOR. Cork production. Updated in septembre 2014, available at URL : [www.apcor.pt/artigo/cork-production.htm]

4. Skidmore Sarah. Stopper pulled on the cork debate. *USA Today* (uploaded in 2007). Available at URL [http://abcnews.go.com/Business/story?id=3525849&page=2]

5. J. McClellan, K. Apples, Corks, and Age. *Blanco County News* (updated in 2014). Available at URL [http://www.blanconews.com/news/116198/]

6. Silva, S. P. *et al.* Cork: properties, capabilities and applications. *Int. Mater. Rev.* **50,** 345–365 (2005).

7. Cooke & B., G. *Cork and the cork tree*. Pergamon Press: USA, 1961.

8. Graça, J. & Pereira, H. Methanolysis of bark suberins: Analysis of glycerol and acid monomers. *Phytochem. Anal.* **11,** 45–51 (2000).

9. Pereira, H. Chemical composition and variability of cork from Quercus suber L. *Wood Sci. Technol.* **22,** 211–218 (1988).

10. Sitte, P. Zum Feinbau der Suberinschichten im Flaschenkork. *Protoplasma* **54,** 555–559 (1962).

11. Cordeiro, N., Belgacem, M. N., Silvestre, A. J. D., Pascoal Neto, C. & Gandini, A. Cork suberin as a new source of chemicals. *Int. J. Biol. Macromol.* **22,** 71–80 (1998).

12. Conde, E. *et al.* Variability of Suberin Composition of Reproduction Cork from Quercus suber Throughout Industrial Processing. *Holzforsch. - Int. J. Macromol.* **53,** 56–62 (2005).

13. Gandini, A., Pascoal Neto, C. & Silvestre, A. J. D. Suberin: A promising renewable resource for novel macromolecular materials. *Prog. Polym. Sci.* **31,** 878–892 (2006).

14. Graça, J. & Santos, S. Suberin: A biopolyester of plants' skin. *Macromol. Biosci.* **7,** 128–135 (2007).

15. Bernards, M. a. Demystifying suberin. *Can. J. Bot.* **80,** 227–240 (2002).

16. Marques, A. V., Pereira, H., Meier, D. & Faix, O. Quantitative Analysis of Cork (Quercus suber L.) and Milled Cork Lignin by FTIR Spectroscopy, Analytical Pyrolysis, and Total Hydrolysis. *Holzforsch. - Int. J. Biol. Chem. Phys. Technol. Wood* **48,** 43–50 (1994).

17. Graça, J. & Pereira, H. Cork Suberin: A Glyceryl Based Polyester. *Holzforschung* **51,** 225–234 (1997).

18. Santos Bento, M. F. *et al.* Study of variability of suberin composition in cork from Quercus suber L. using thermally assisted transmethylation GC-MS. *J. Anal. Appl. Pyrolysis* **57,** 45–55 (2001).

19. Bernards, M. & Lewis, N. G. The macromolecular aromatic domain in suberized tissue: A changing paradigm. *Phytochemistry* **47,** 915–933 (1998).

20. Zeier, J. & Schreiber, L. Comparative investigation of primary and tertiary endodermal cell walls isolated from the roots of five monocotyledoneous species: Chemical composition in relation to fine structure. *Planta* **206,** 349–361 (1998).

21. Schreiber, L., Hartmann, K., Skrabs, M. & Zeier, J. Apoplastic barriers in roots: chemical composition of endodermal and hypodermal cell walls. *J. Exp. Bot.* **50,** 1267–1280 (1999).

22. Zimmermann, H. M., Hartmann, K., Schreiber, L. & Steudle, E. Chemical composition of apoplastic transport barriers in relation to radial hydraulic conductivity of corn roots (Zea mays L.). *Planta* **210,** 302–311 (2000).

23. Gil, A. ., Lopes, M., Rocha, J. & Pascoal Neto, C. A 13C solid state nuclear magnetic resonance spectroscopic study of cork cell wall structure: the effect of suberin removal. *Int. J. Biol. Macromol.* **20,** 293–305 (1997).

24. Lopes, M. H., Gil, A. M., Silvestre, A. J. D. & Neto, C. P. Composition of suberin extracted upon gradual alkaline methanolysis of Quercus suber L. Cork. *J. Agric. Food Chem.* **48,** 383–391 (2000).

25. Lewis, N. G. A 20th century roller coaster ride: A short account of lignification. *Curr. Opin. Plant Biol.* **2,** 153–162 (1999).

26. Velings, N. M. & Mestdagh, M. M. Protein Adsorption in Calcium Alginate Gel Beads. *J. Bioact. Compat. Polym.* **9,** 133–141 (1994).

27. Brun, N., Ungureanu, S., Deleuze, H. & Backov, R. Hybrid foams, colloids and beyond: from design to applications. *Chem. Soc. Rev.* **40,** 771–788 (2011).

28. Kistler, S. S. Coherent Expanded Aerogels and Jellies. *Nature* **127,** 741 (1931).

29. Roth, K. Delikate grenzflächen teil: Von der sauce vinaigrette zur mayonnase. *Chemie Unserer Zeit* **42,** 160–172 (2008).

30. Léal-Calderon, Schmitt, V. & Bibette, J. *Emulsion Science: Basic principle*. (2007).

31. Asua, J. M. Challenges for industrialization of miniemulsion polymerization. *Prog. Polym. Sci.* **39,** 1797–1826 (2014).

32. Ramsden, W. Separation of solids in the surface-layers of solutions and ‘suspensions’No Title. *Proc. R. Soc. London* **72,** 156–164 (1903).

33. Pickering, S. U., *Pickering : Emulsions.* 2001–2021 (1907).

34. Rayner, M. *et al.* Biomass-based particles for the formulation of Pickering type emulsions in food and topical applications. *Colloids Surfaces A* **458,** 48–62 (2014).

35. Voronov, S., Kohut, A., Tarnavchyk, I. & Voronov, A. Advances in reactive polymeric surfactants for interface modification. *Curr. Opin. Colloid* **19,** 95–121 (2014).

36. Odian, G. in *Principles of Polymerization* (John Wiley & Sons, 2004).

37. Blaker, J. J., Lee, K.-Y., Li, X., Menner, A. & Bismarck, A. Renewable nanocomposite polymer foams synthesized from Pickering emulsion templates. *Green Chem.* **11,** 1321 (2009).

38. Cunha, A. G., Mougel, J. B., Cathala, B., Berglund, L. A. & Capron, I. Preparation of double pickering emulsions stabilized by chemically tailored nanocelluloses. *Langmuir* **30,** 9327–9335 (2014).

39. Ikem, V. O., Menner, A. & Bismarck, A. High internal phase emulsions stabilized solely by functionalized silica particles. *Angew. Chemie - Int. Ed.* **47,** 8277–8279 (2008).

40. Tasset, S., Cathala, B., Bizot, H. & Capron, I. Versatile cellular foams derived from CNC-stabilized Pickering emulsions. *RSC Adv.* **4,** 893 (2014).

41. Trovatti, E., Serafim, L. S., Freire, C. S. R., Silvestre, A. J. D. & Neto, C. P. Gluconacetobacter sacchari: An efficient bacterial cellulose cell-factory. *Carbohydr. Polym.* **86,** 1417–1420 (2011).

42. Carreira, P., Mendes, J. S., Trovatti, E., Serafim, L. S., Freire, C. S R, Silvestre, A. J. D., Neto, C. P., Utilization of residues from agro-forest industries in the production of high value bacterial cellulose. *Bioresour. Technol.* **102,** 7354–7360 (2011).

43. Hestrin, S. & Schramm, M. Synthesis of cellulose by Acetobacter xylinum. 2. Preparation of freeze-dried cells capable of polymerizing glucose to cellulose*. *Biochem. J.* **58,** 345–352 (1954).

44. Tomé, L. C. Pinto, Ricardo J. B., Trovatti, E., Freire, C. S. R.,Silvestre, A. J. D., Neto, C. P., Gandini, A. Transparent bionanocomposites with improved properties prepared from acetylated bacterial cellulose and poly(lactic acid) through a simple approach. *Green Chem.* **13,** 419 (2011).

45. López, S. & Santiago, E. Acrylated-Epoxidized Soybean Oil-Based Polymers and Their Use in the Generation of Electrically Conductive Polymer Composites. *Intech* 231–263 (2013).

46. Coates, J. Interpretation of Infrared Spectra, A Practical Approach. *Encycl. Anal. Chem.* 10815–10837 (2000).

47. Lee, K., Blaker, J. J. & Murakami, R. Phase Behavior of Medium and High Internal Phase Water-in-Oil Emulsions Stabilized Solely by Hydrophobized Bacterial Cellulose Nano fibrils. *Langmuir* **30,** 452–460 (2014).

48. Ikem, V. O., Menner, A., Horozov, T. S. & Bismarck, A. Highly permeable macroporous polymers synthesized from pickering medium and high internal phase emulsion templates. *Adv. Mater.* **22,** 3588–3592 (2010).

49. Pelletier, H., Belgacem, N. & Gandini, A. Acrylated vegetable oils as photocrosslinkable materials. *J. Appl. Polym. Sci.* **99,** 3218–3221 (2006).

50. Mir, a., Bezzazi, B., Zitoune, R. & Collombet, F. Study of mechanical and hygrothermal properties of agglomerated cork. *Mechanika* **18,** 40–45 (2012).

51. Kass, M. D., Theiss, T. J., Janke, C. J. & Pawel, S. J. *Compatibility study for plastic, elastomeric , and metallic fueling infrastructure materials exposed ethanol-blendedgasoline*. Oak bridge National Laboratory journal, (2012).

52. MANO J. F. The Viscoelastic Properties of Cork. *J. Mater. Sci.* **37,** 257–263 (2002).

53. Chaiyasat, P. Preparation and Characterization of Poly(divinylbenzene) Microcapsules Containing Octadecane. *Mater. Sci. Appl.* **02,** 1007–1013 (2011).

54. Cummings, B. *Biology: concepts and connections*. Pearson: New York, 2008.